Deep Learning for Remote Sensing

Yonghao Xu
Computer Vision Laboratory
Department of Electrical Engineering
Linköping University

Sensing without physical contact

Source credit: ESA

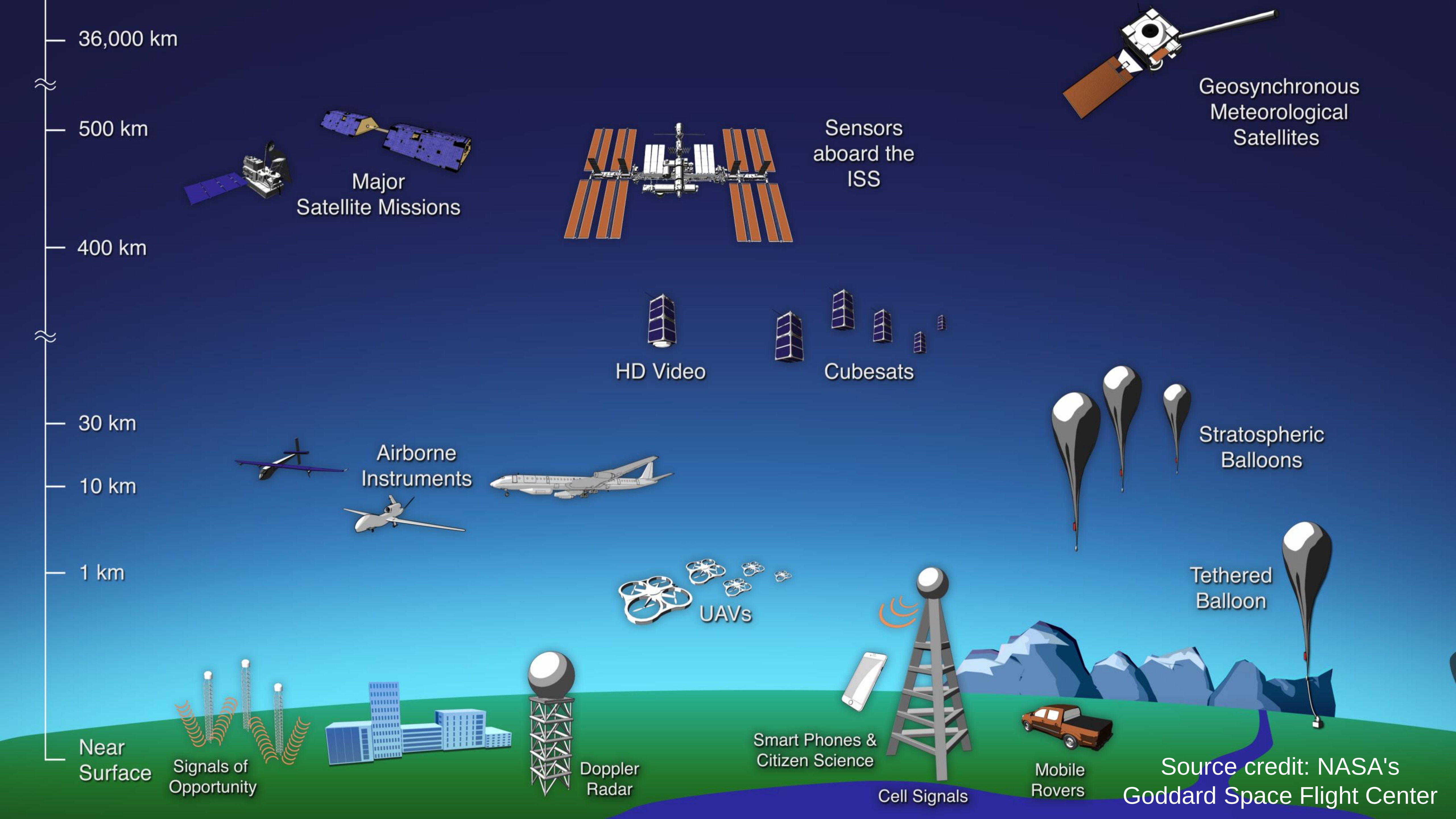

Source credit: NASA's Goddard Space Flight Center


Middelgrunden, Denmark
1984
Google Earth Timelapse

From Data to Information

Land Cover Mapping

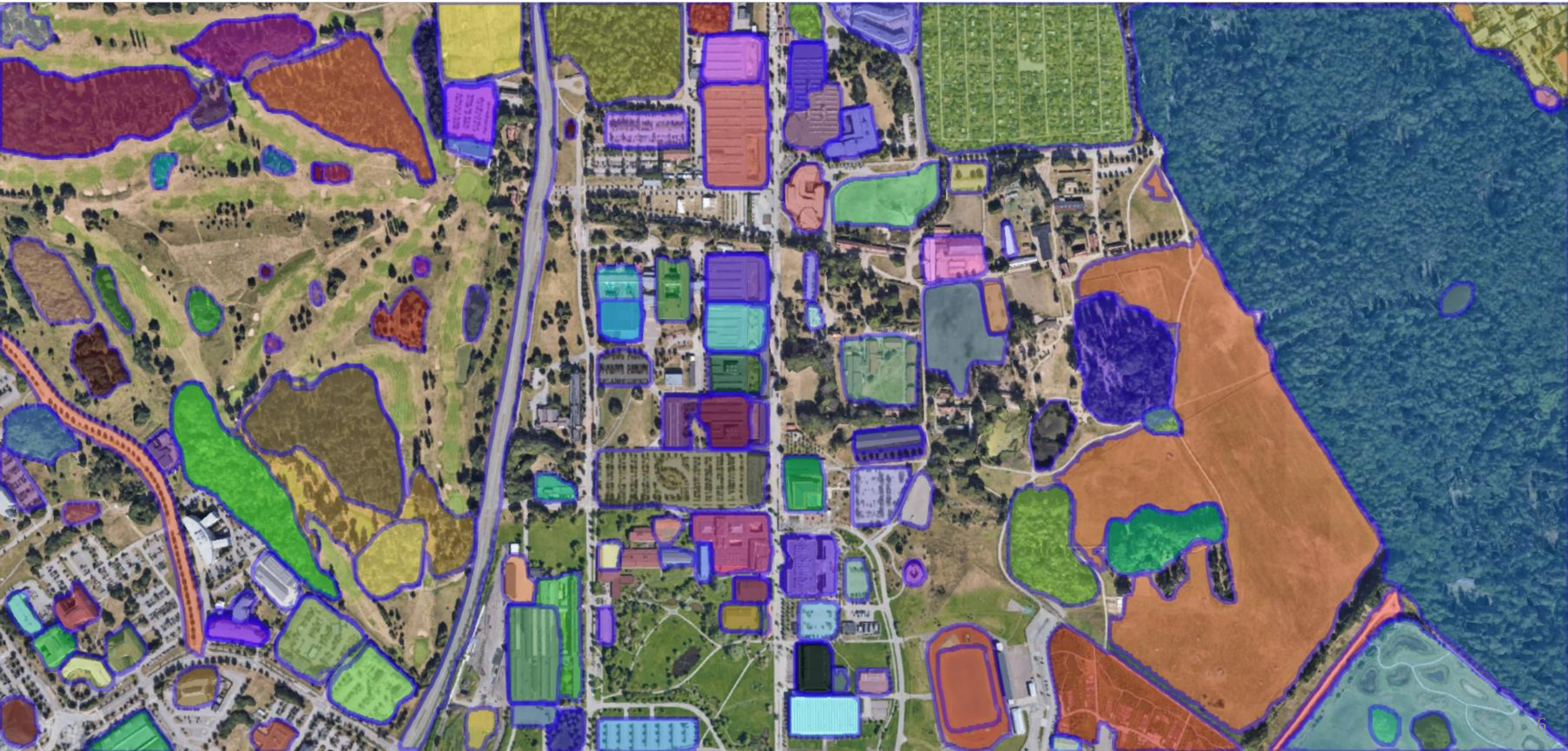

AI-Driven Remote Sensing Data Interpretation

- Data in and insights out

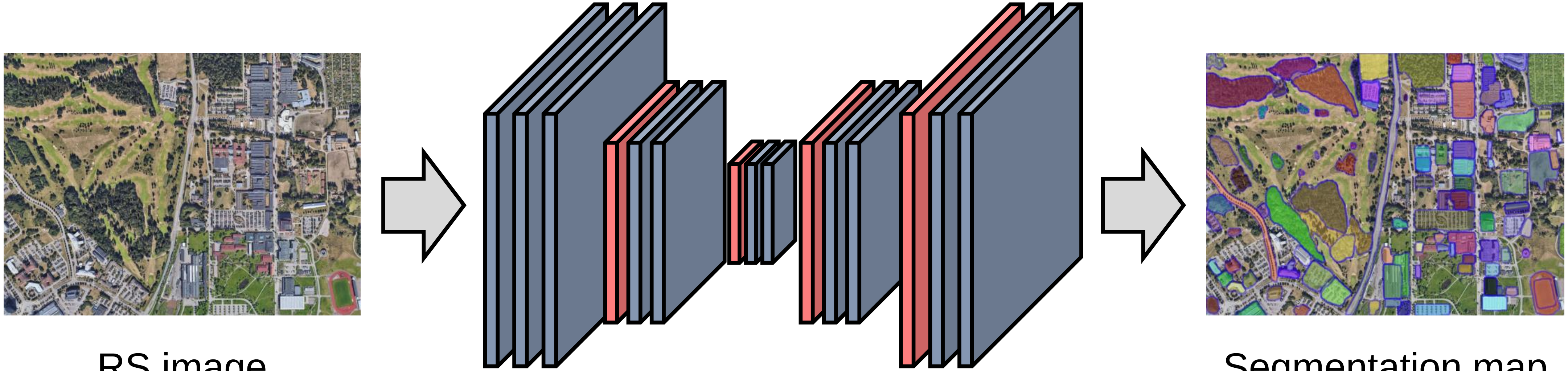

RS image

Segmentation map

Deep neural network

AI-Driven Remote Sensing Data Interpretation

- Data in and insights out

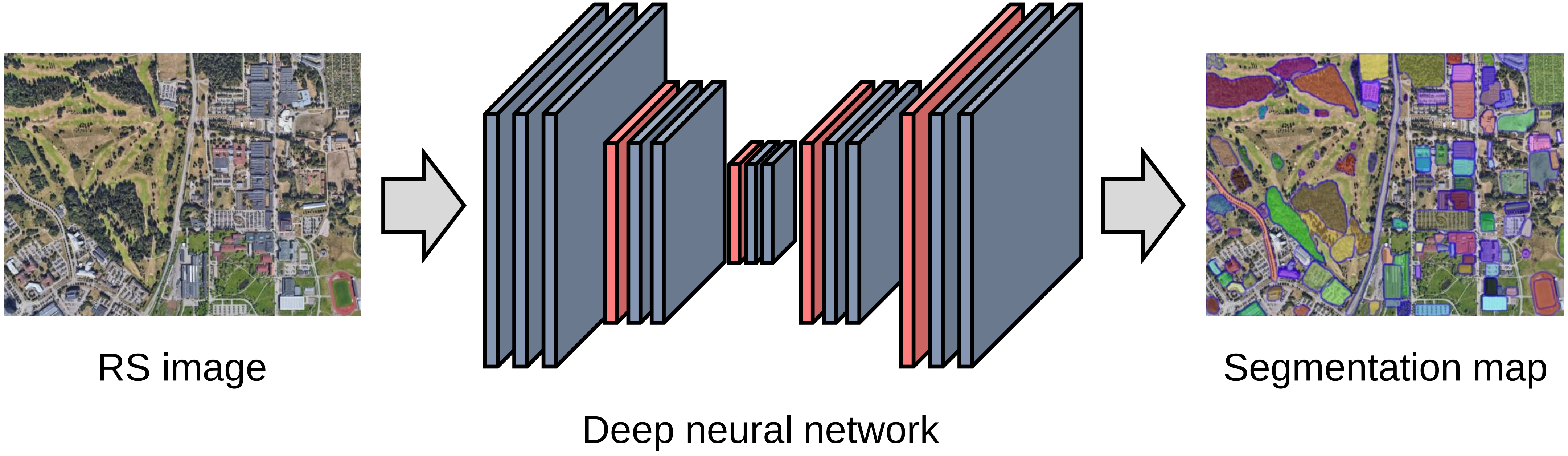

- Challenge

Deep neural networks are **data-hungry**

The collection of high-quality annotations is **time-consuming**!

Unsupervised Learning

- Spectrum data synthesis with GAN

$$\min_G \max_D V(D,G) = \mathrm{E}_{x\sim p_x(x)} \log D(x|y) + \mathrm{E}_{z\sim p_z(z)} \log\left(1 - D(G(z|y))\right)$$

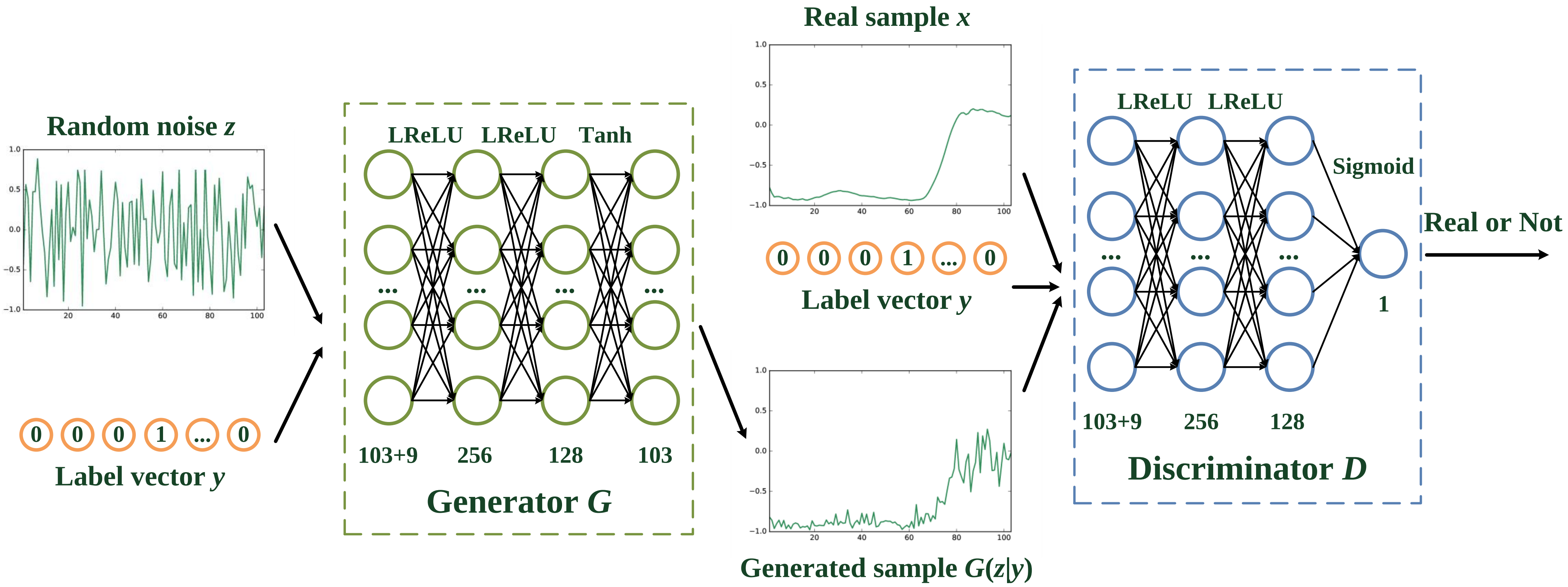

Y. Xu, B. Du, and L. Zhang, "Can we generate good samples for hyperspectral classification?—A generative adversarial network based method," in *Proc. IEEE Int. Geosci. Remote Sens. Symp.*, 2018.

Unsupervised Learning

- Spectrum data synthesis with GAN

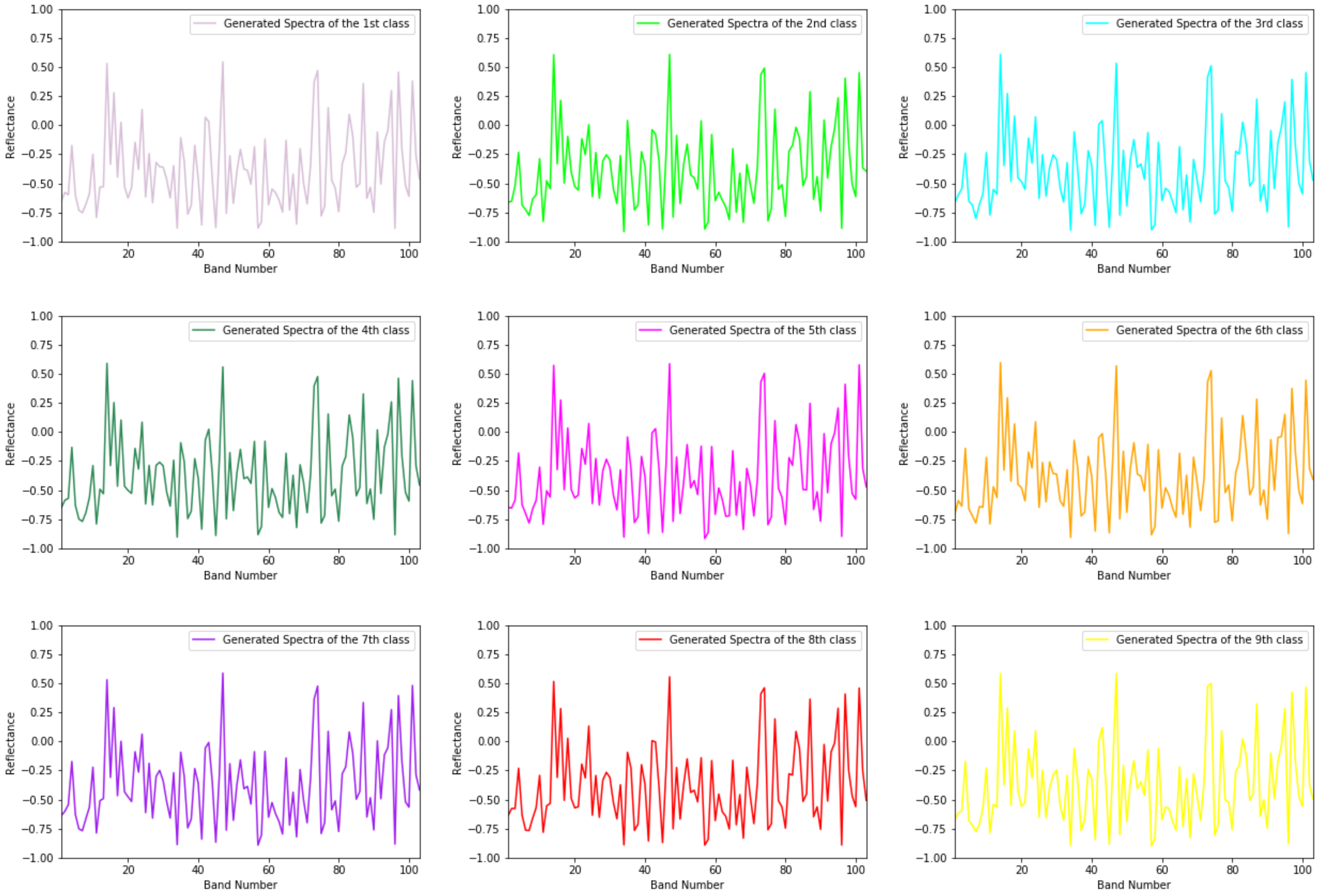

The first 100 wavebands are reshaped into a 10×10 image for visualization

Y. Xu, B. Du, and L. Zhang, "Can we generate good samples for hyperspectral classification?—A generative adversarial network based method," in *Proc. IEEE Int. Geosci. Remote Sens. Symp.*, 2018.

Semi-supervised Learning

- Learning with unlabeled data

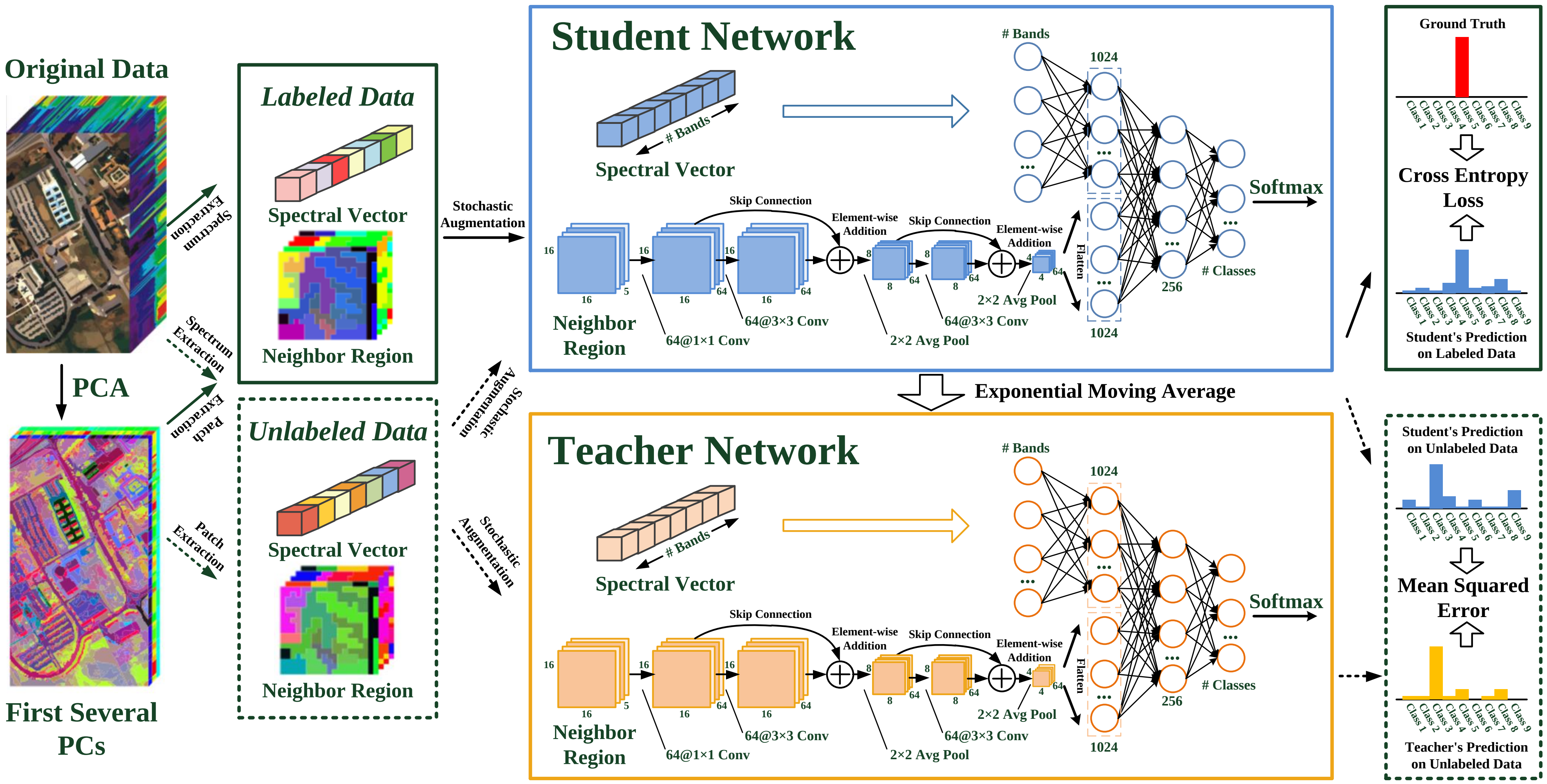

Y. Xu, B. Du, and L. Zhang, "Robust self-ensembling network for hyperspectral image classification," in *IEEE Trans. Neural Netw. Learn. Syst.*, vol. 35, no. 3, pp. 3780-3793, 2022.

Semi-supervised Learning

- Performance of teacher and student nets over time

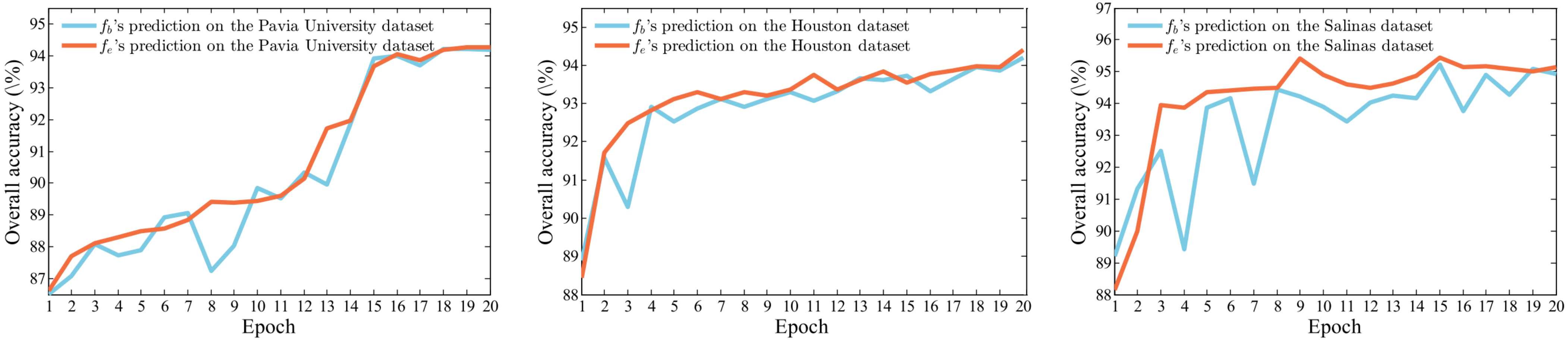

Y. Xu, B. Du, and L. Zhang, "Robust self-ensembling network for hyperspectral image classification," in *IEEE Trans. Neural Netw. Learn. Syst.*, vol. 35, no. 3, pp. 3780-3793, 2022.

Semi-supervised Learning

- Performance of teacher and student nets over time

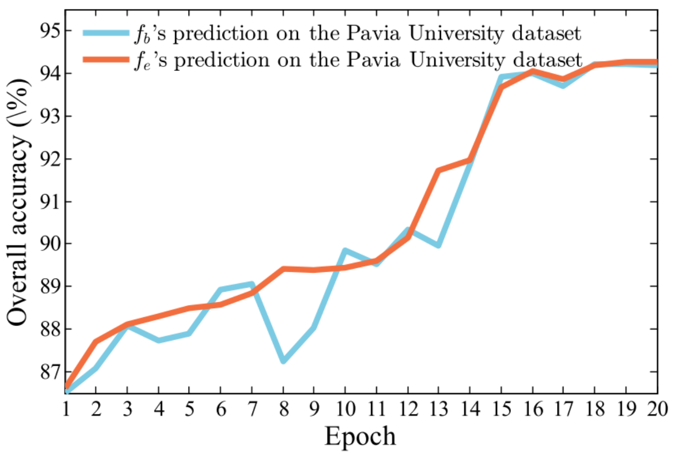

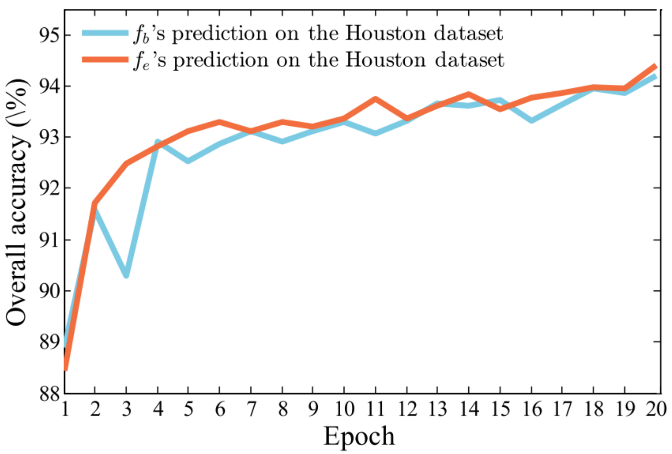

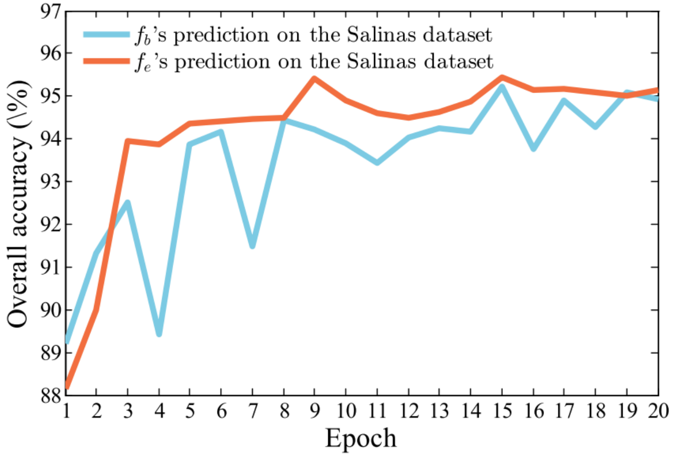

- Performance with different numbers of unlabeled samples

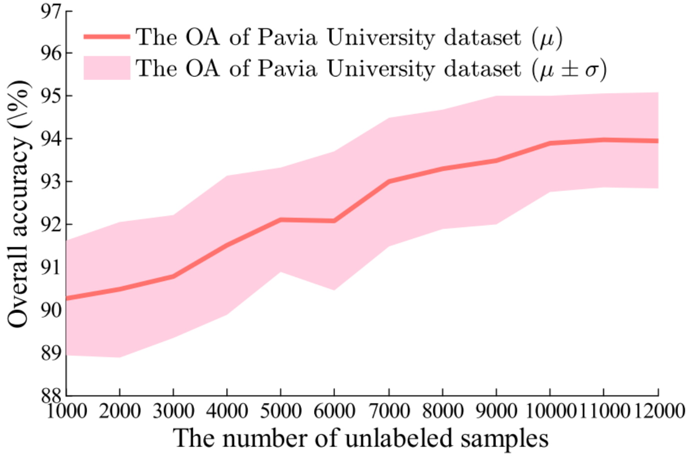

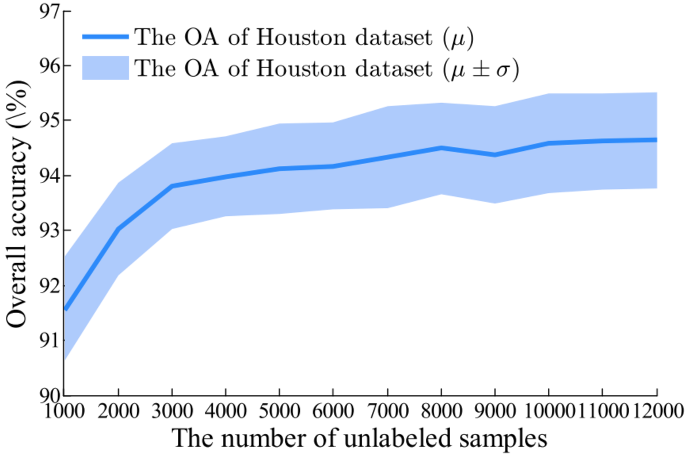

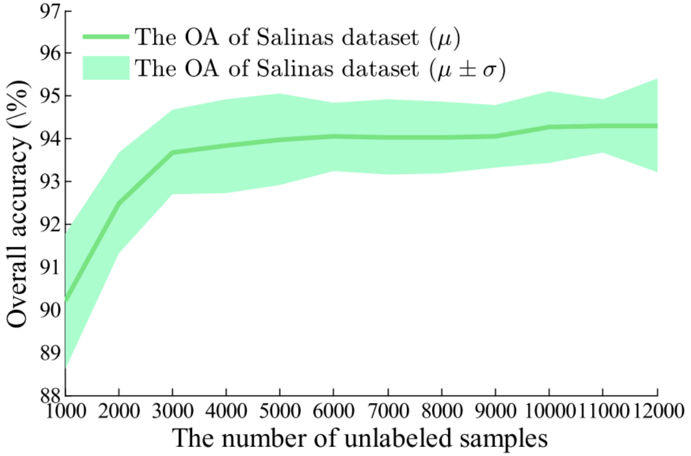

Y. Xu, B. Du, and L. Zhang, "Robust self-ensembling network for hyperspectral image classification," in *IEEE Trans. Neural Netw. Learn. Syst.*, vol. 35, no. 3, pp. 3780-3793, 2022.

Weakly Supervised Learning

- Reduce the annotation burden?

VHR image

Point-level annotations

Dense annotations

Y. Xu and P. Ghamisi, “Consistency-regularized region-growing network for semantic segmentation of urban scenes with point-level annotations,” *IEEE Trans. Image Process.*, vol. 31, pp. 5038–5051, 2022.

Weakly Supervised Learning

- The spatial continuity of ground objects:

  Adjacent pixels are likely to belong to the same category

VHR image

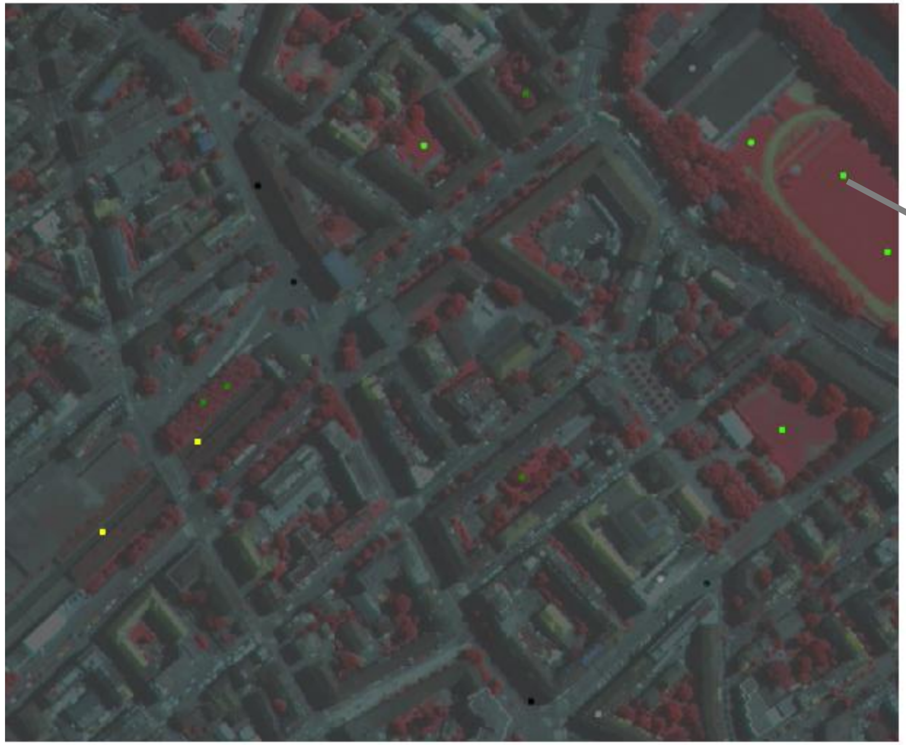

Point-level annotations

8-connectivity neighborhood

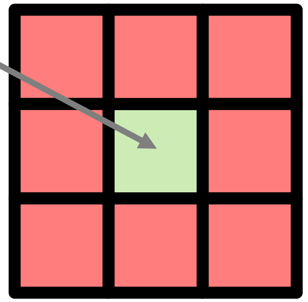

Neighborhood pixels are likely to belong to the grass

Y. Xu and P. Ghamisi, "Consistency-regularized region-growing network for semantic segmentation of urban scenes with point-level annotations," *IEEE Trans. Image Process.*, vol. 31, pp. 5038–5051, 2022.

Weakly Supervised Learning

- Consistency-regularized region-growing network

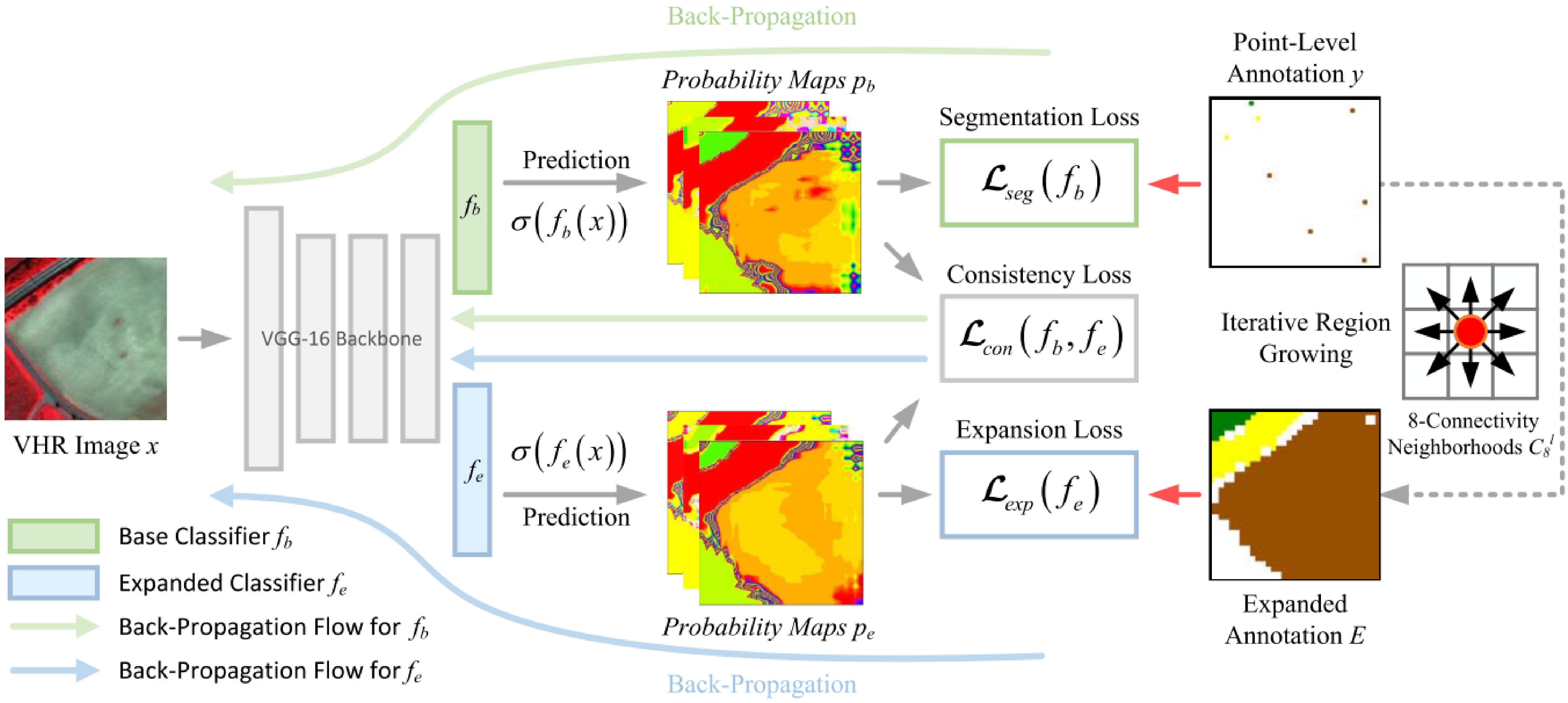

Y. Xu and P. Ghamisi, "Consistency-regularized region-growing network for semantic segmentation of urban scenes with point-level annotations," *IEEE Trans. Image Process.*, vol. 31, pp. 5038–5051, 2022.

Weakly Supervised Learning

- Region Growing

Segmentation loss for the base classifier: $$\mathcal{L}_{seg}\left(f_b\right) = -\frac{1}{n}\sum_{i=1}^{n}\sum_{c=1}^{k} y^{(i,c)} \log\left(p_b^{(i,c)}\right)$$

Initialize ***E*** with the original point-level label ***y***: $$E^{(i)} = \arg\max_c y^{(i,c)}$$

For each labeled pixel ***l***, visit the unlabeled pixel ***u*** in its corresponding 8-connectivity neighborhood regions

$$E^{(u)} \leftarrow E^{(l)},\ if\ \begin{cases} \arg\max_c \left(p_b^{(u,c)}\right) = E^{(l)} \\ p_b^{\left(u,E^{(l)}\right)} \geq \tau, \end{cases}$$

Weakly Supervised Learning

- Consistency Regularization

Expansion loss:

$$J_c\left(\tilde{E}, E\right) = \frac{\left|\{\tilde{E}=c\} \cap \{E=c\}\right|}{\left|\{\tilde{E}=c\} \cup \{E=c\}\right|} \qquad \Delta_{J_c}\left(\tilde{E}, E\right) = 1 - J_c\left(\tilde{E}, E\right)$$

(Lovasz softmax loss)

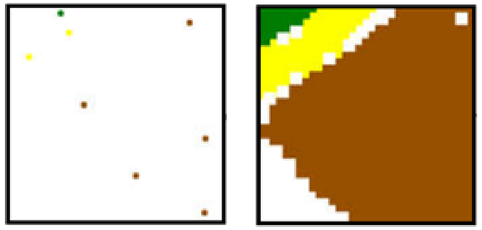

$$M^{(i,c)} = \begin{cases} 1 - p_e^{(i,c)} & if\ c = E^{(i)} \\ p_e^{(i,c)} & if\ c \neq E^{(i)} \end{cases} \qquad \mathcal{L}_{exp}\left(f_e\right) = -\frac{1}{n}\sum_{i=1}^{n}\sum_{c=1}^{k}\overline{\Delta_{J_c}}\left(M^{(i,c)}\right)$$

Consistency regularization loss:

$$\mathcal{L}_{con}\left(f_b, f_e\right) = -\frac{1}{n}\sum_{i=1}^{n}\sum_{c=1}^{k}\|p_b^{(i,c)} - p_e^{(i,c)}\|^2$$

Full loss function:

$$\mathcal{L}\left(f_b, f_e\right) = \mathcal{L}_{seg}\left(f_b\right) + \mathcal{L}_{exp}\left(f_e\right) + \lambda_{con}\mathcal{L}_{con}\left(f_b, f_e\right)$$

LINKÖPING UNIVERSITY ELLIIT Excellence Center at Linköping – Lund in Information Technology

Weakly Supervised Learning

- Dynamically expanded annotations at different iterations

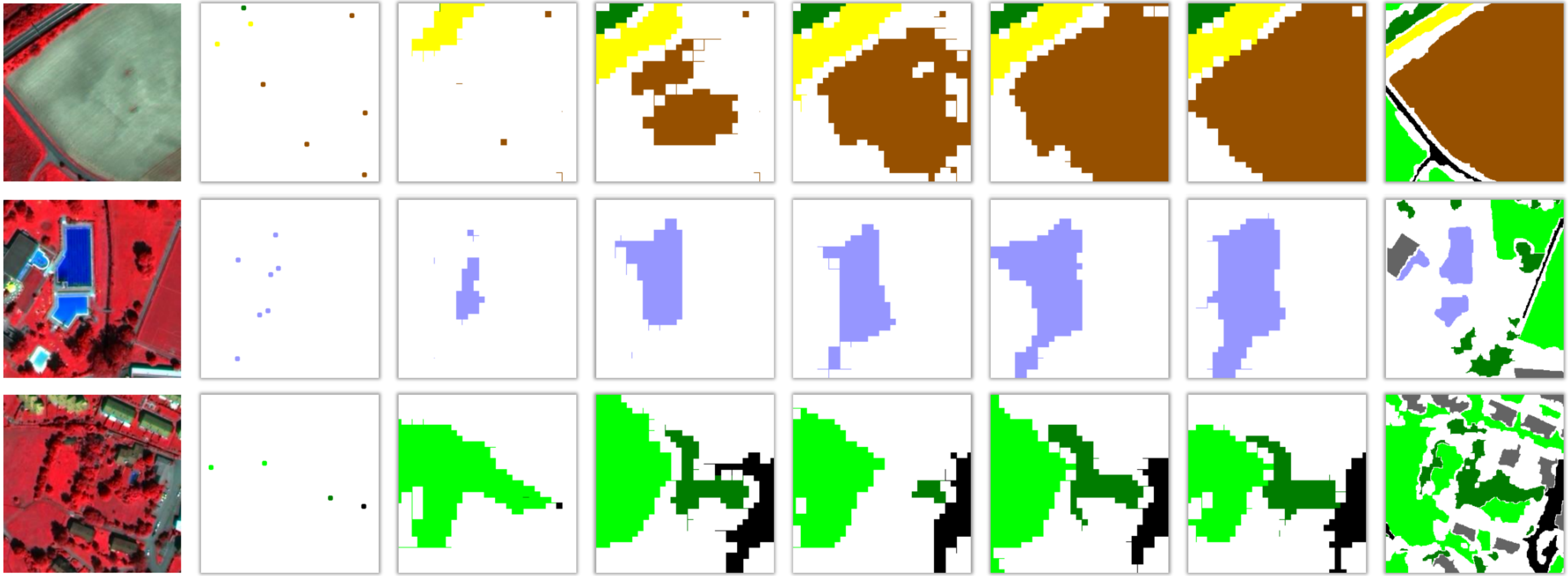

VHR image | Point-level annotations | Iter #100 | Iter #200 | Iter #300 | Iter #400 | Iter #500 | Pixel-wise annotations

Y. Xu and P. Ghamisi, “Consistency-regularized region-growing network for semantic segmentation of urban scenes with point-level annotations,” *IEEE Trans. Image Process.*, vol. 31, pp. 5038–5051, 2022.

LINKÖPING UNIVERSITY ELLIIT Excellence Center at Linköping – Lund in Information Technology

AI-Driven Remote Sensing Data Interpretation

- Challenge: Deep neural networks are **data-hungry**
  - ✓ Developing specially designed machine learning algorithms
    - Unsupervised learning
    - Semi-supervised learning
    - Weakly supervised learning
    - ……

LINKÖPING UNIVERSITY ELLIIT Excellence Center at Linköping – Lund in Information Technology

AI-Driven Remote Sensing Data Interpretation

- Challenge: Deep neural networks are **data-hungry**
  - ✓ Developing specially designed machine learning algorithms
    - Unsupervised learning
    - Semi-supervised learning
    - Weakly supervised learning
    - ……
  - ✓ Collecting high-quality annotated benchmark datasets

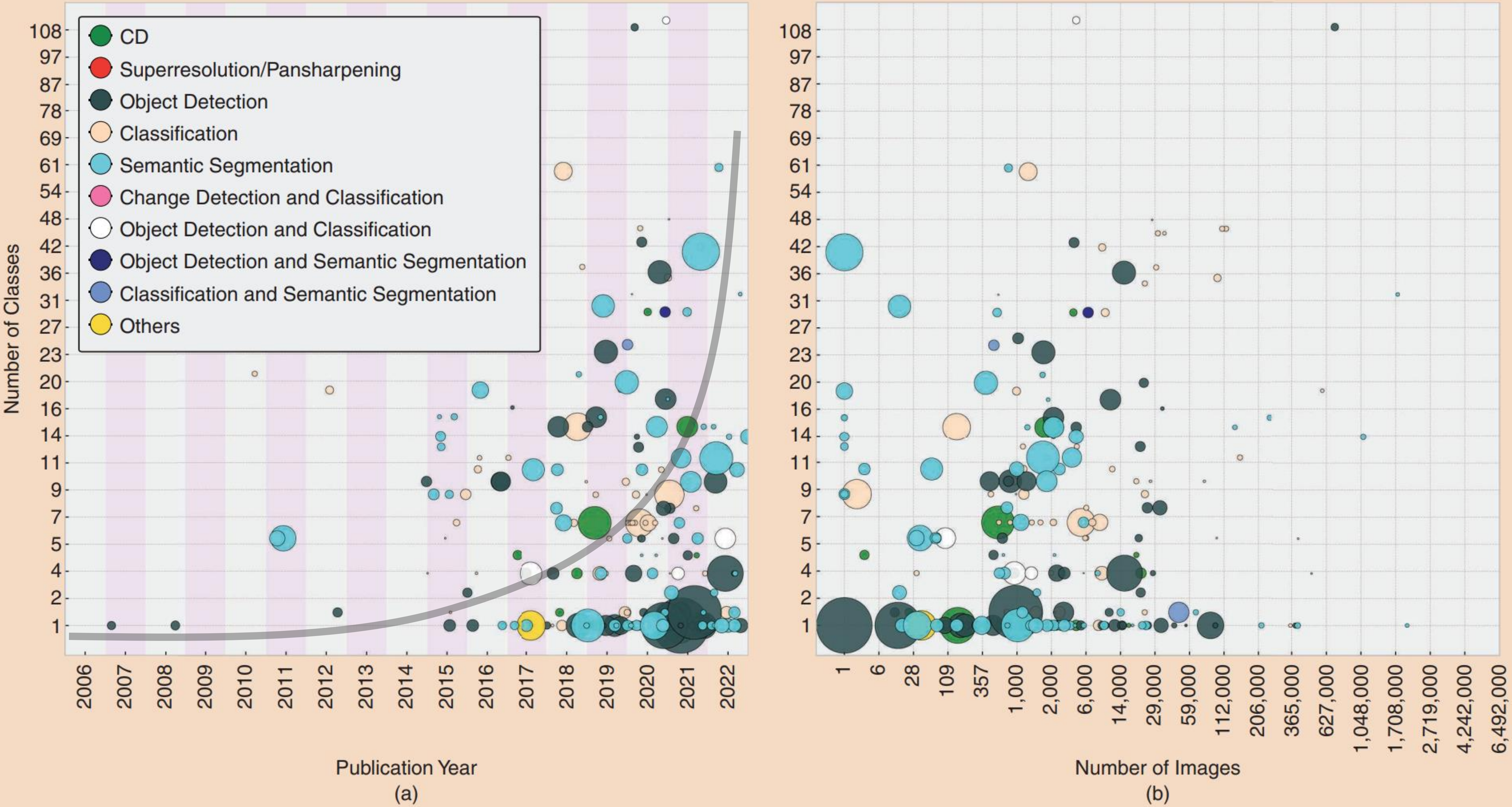

LINKÖPING UNIVERSITY ELLIIT Excellence Center at Linköping – Lund in Information Technology

M. Schmitt, S. Ahmadi, Y. Xu, G. Taşkin, U. Verma, F. Sica, and R. Hänsch, "There are no data like more data: Datasets for deep learning in earth observation," *IEEE Geosci. Remote Sens. Mag.*, vol. 11, no. 3, pp. 63-97, 2023.

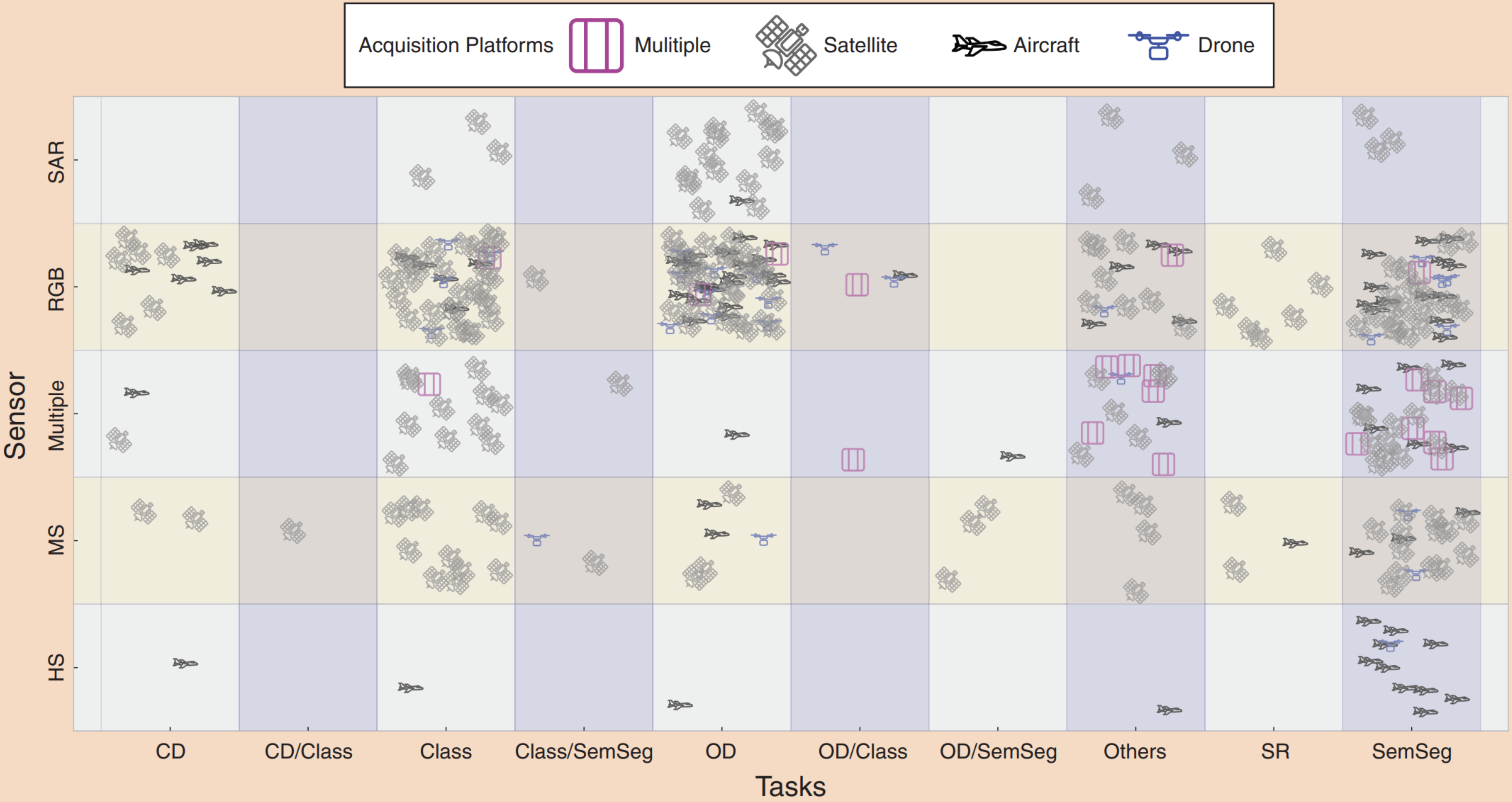

M. Schmitt, S. Ahmadi, Y. Xu, G. Taşkin, U. Verma, F. Sica, and R. Hänsch, "There are no data like more data: Datasets for deep learning in earth observation," *IEEE Geosci. Remote Sens. Mag.*, vol. 11, no. 3, pp. 63-97, 2023.

Data Fusion

- Advantages of different types of RS data
  - Hyperspectral image: Rich spectral information
  - Very high-resolution image: Precise spatial details
  - LiDAR data: Elevation information

Data Fusion

- Advantages of different types of RS data
  - Hyperspectral image: Rich spectral information
  - Very high-resolution image: Precise spatial details
  - LiDAR data: Elevation information

HSI

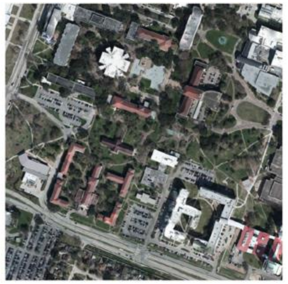

VHRI

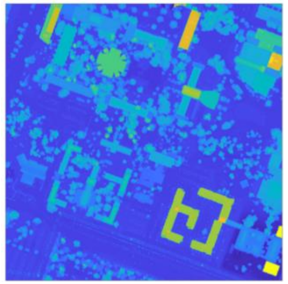

LiDAR

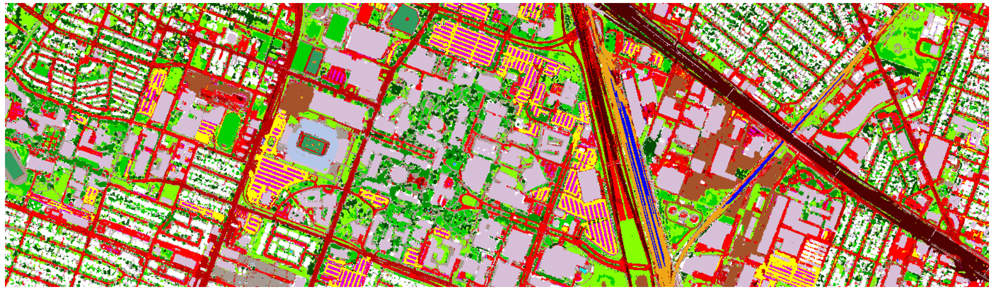

Multi-sensor land cover mapping

Y. Xu, B. Du, L. Zhang, D. Cerra, et al., “Advanced multi-sensor optical remote sensing for urban land use and land cover classification: Outcome of the 2018 IEEE GRSS Data Fusion Contest,” in *IEEE J. Sel. Top. Appl. Earth Obs. Remote Sens.*, vol. 12, no. 6, pp. 1709-1724, 2019.

Data Fusion

Training (red) and test (entire imagery except red) areas

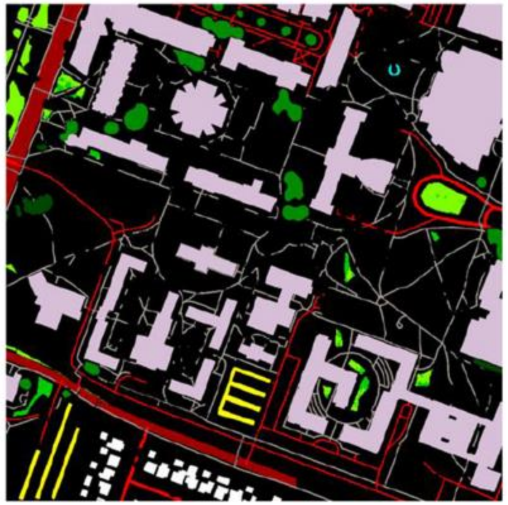

GT

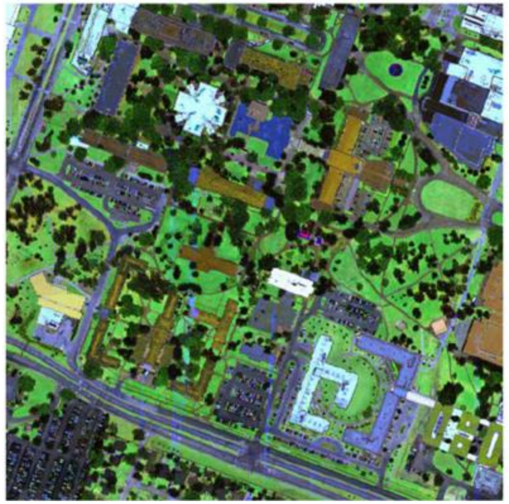

Multispectral LiDAR

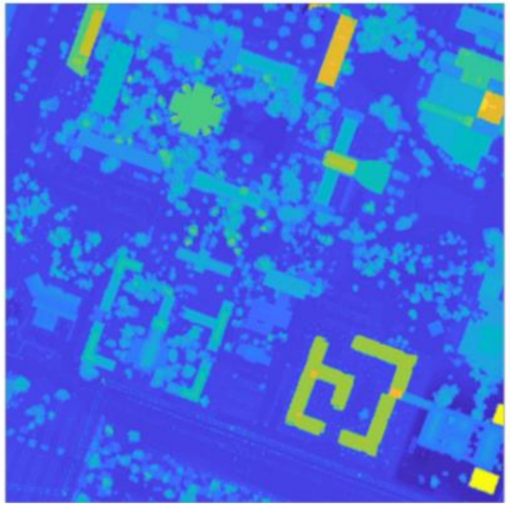

DSM

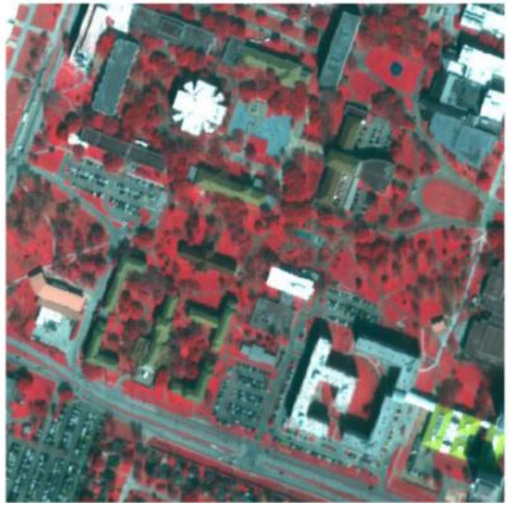

HSI

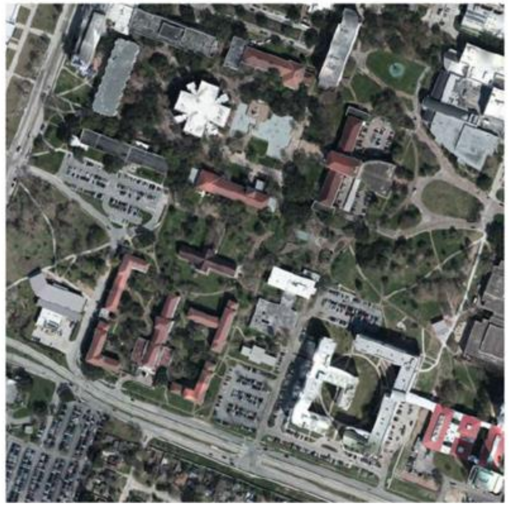

VHR

Y. Xu, B. Du, L. Zhang, D. Cerra, et al., “Advanced multi-sensor optical remote sensing for urban land use and land cover classification: Outcome of the 2018 IEEE GRSS Data Fusion Contest,” in *IEEE J. Sel. Top. Appl. Earth Obs. Remote Sens.*, vol. 12, no. 6, pp. 1709-1724, 2019.

Data Fusion

- End-to-end network

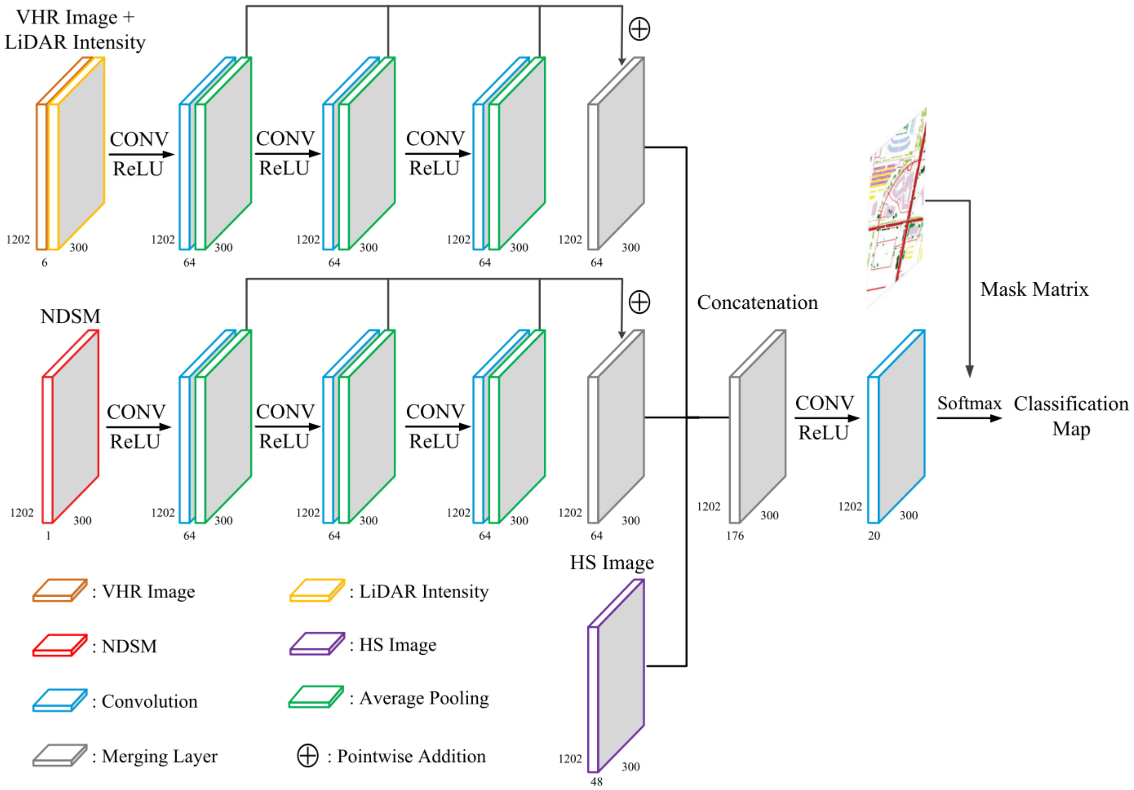

Fusion-FCN

(1st place in IEEE Data Fusion Contest 2018)

Y. Xu, B. Du, L. Zhang, D. Cerra, et al., “Advanced multi-sensor optical remote sensing for urban land use and land cover classification: Outcome of the 2018 IEEE GRSS Data Fusion Contest,” in *IEEE J. Sel. Top. Appl. Earth Obs. Remote Sens.*, vol. 12, no. 6, pp. 1709-1724, 2019.

Data Fusion

- End-to-end network
- Base classifier + detectors

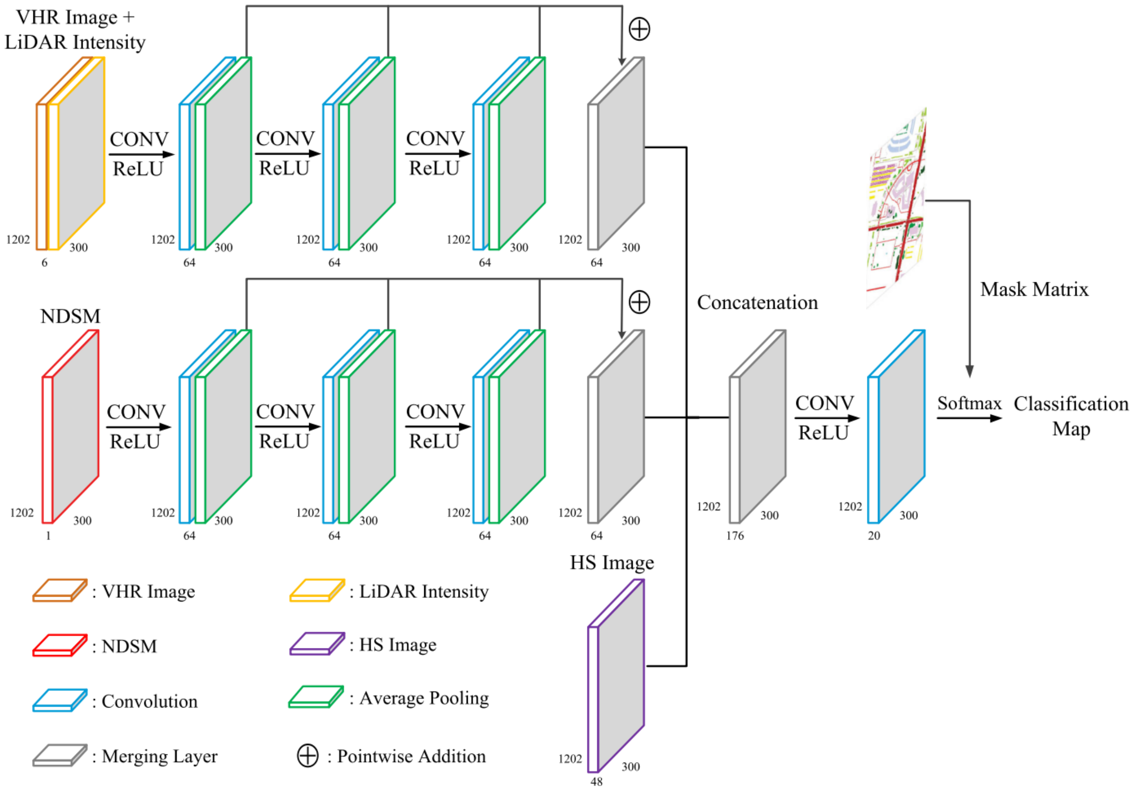

Fusion-FCN

(1st place in IEEE Data Fusion Contest 2018)

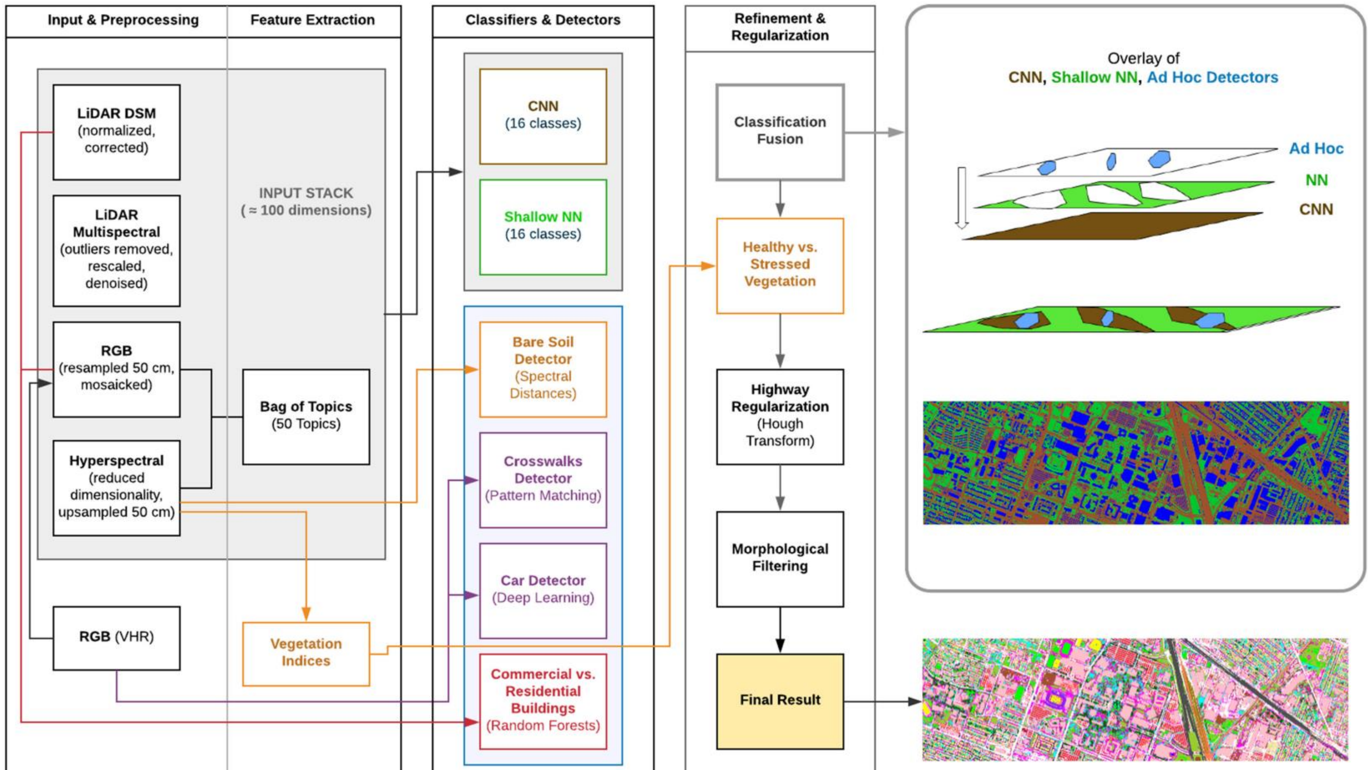

Ensemble with ad hoc detectors

(2nd place in IEEE Data Fusion Contest 2018)

Y. Xu, B. Du, L. Zhang, D. Cerra, et al., “Advanced multi-sensor optical remote sensing for urban land use and land cover classification: Outcome of the 2018 IEEE GRSS Data Fusion Contest,” in *IEEE J. Sel. Top. Appl. Earth Obs. Remote Sens.*, vol. 12, no. 6, pp. 1709-1724, 2019.

AI Security

- Are deep neural networks robust to perturbation?

Airplane

Perturbation

Runway

96.56% confidence

Storage tanks

Perturbation

Intersection

99.99% confidence

Y. Xu, B. Du, and L. Zhang, "Assessing the threat of adversarial examples on deep neural networks for remote sensing scene classification: Attacks and defenses," *IEEE Trans. Geosci. Remote. Sens.*, vol. 59, no. 2, pp. 1604–1617, 2021.

AI Security

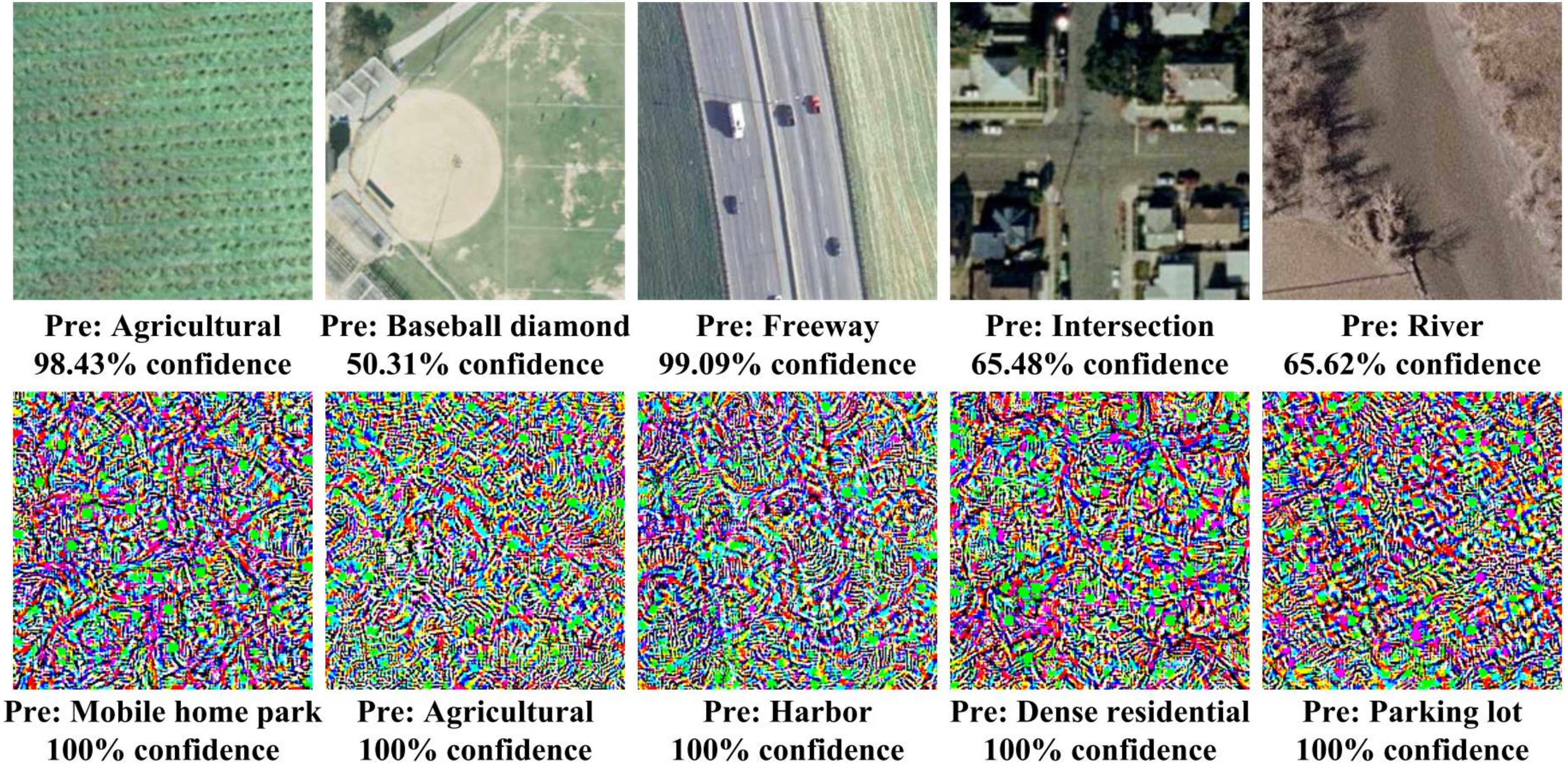

Y. Xu, B. Du, and L. Zhang, "Assessing the threat of adversarial examples on deep neural networks for remote sensing scene classification: Attacks and defenses," *IEEE Trans. Geosci. Remote. Sens.*, vol. 59, no. 2, pp. 1604–1617, 2021.

AI Security

- Are deep neural networks robust to perturbation?

Adversarial patch on the roof of a car

Without adversarial patches

Adversarial patch off-and-around a car

With adversarial patches

Du, A., Chen, B., Chin, T.J., Law, Y.W., Sasdelli, M., Rajasegaran, R. and Campbell, D., Physical adversarial attacks on an aerial imagery object detector. In *WACV*, 2022.

UAE-RS Dataset

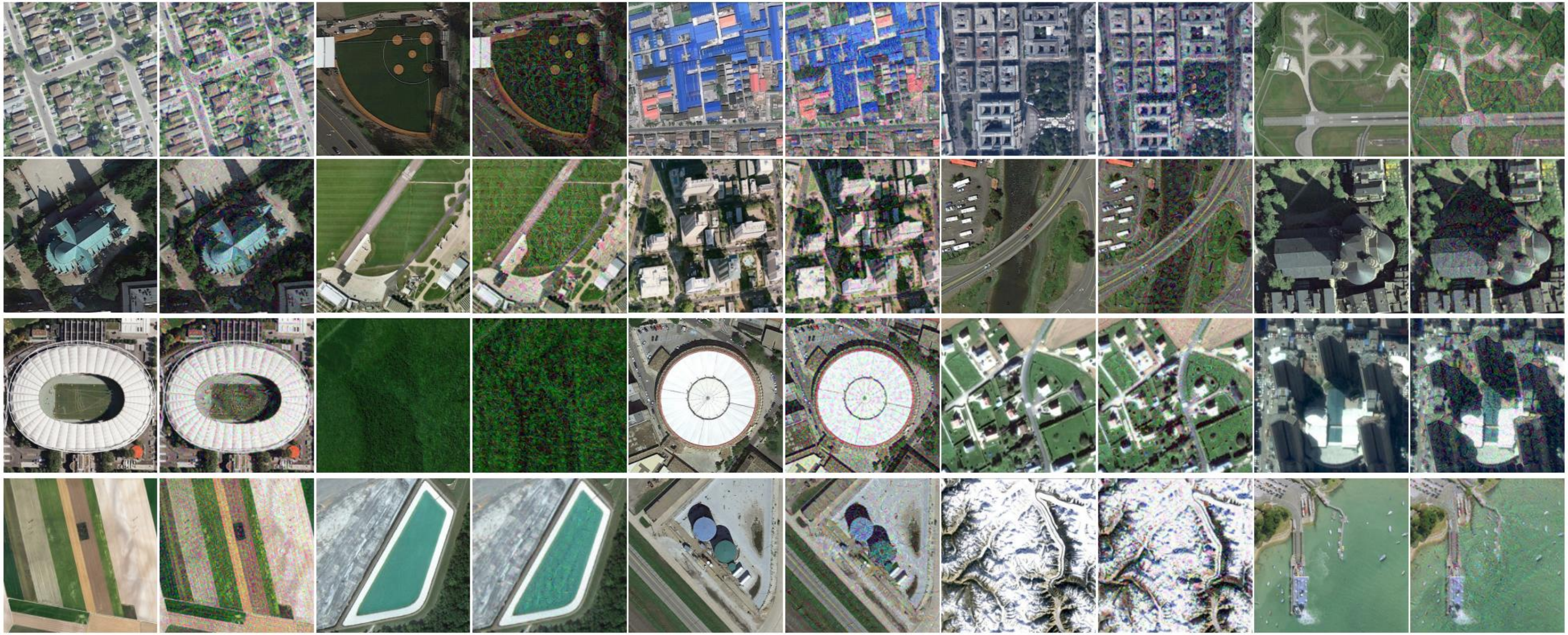

Example images in the AID dataset and the corresponding adversarial examples in the UAE-RS dataset

Y. Xu and P. Ghamisi, "Universal adversarial examples in remote sensing: Methodology and benchmark," *IEEE Trans. Geosci. Remote Sens.*, vol. 60, pp. 1−15, 2022.

Quantitative Results on UAE-RS Dataset

QUANTITATIVE SCENE CLASSIFICATION RESULTS OF DIFFERENT DEEP NEURAL NETWORKS ON THE CLEAN AND UAE-RS TEST SETS.

Model	UCM Clean Test Set	UCM UAE-RS Test Set	UCM OA Gap	AID Clean Test Set	AID UAE-RS Test Set	AID OA Gap
AlexNet [48]	90.28	30.86	-59.42	89.74	18.26	-71.48
VGG11 [56]	94.57	26.57	-68.00	91.22	12.62	-78.60
VGG16 [56]	93.04	19.52	-73.52	90.00	13.46	-76.54
VGG19 [56]	92.85	29.62	-63.23	88.30	15.44	-72.86
Inception-v3 [57]	96.28	24.86	-71.42	92.98	23.48	-69.50
ResNet18 [49]	95.90	2.95	-92.95	94.76	0.02	-94.74
ResNet50 [49]	96.76	25.52	-71.24	92.68	6.20	-86.48
ResNet101 [49]	95.80	28.10	-67.70	92.92	9.74	-83.18
ResNeXt50 [58]	97.33	26.76	-70.57	93.50	11.78	-81.72
ResNeXt101 [58]	97.33	33.52	-63.81	95.46	12.60	-82.86
DenseNet121 [50]	97.04	17.14	-79.90	95.50	10.16	-85.34
DenseNet169 [50]	97.42	25.90	-71.52	95.54	9.72	-85.82
DenseNet201 [50]	97.33	26.38	-70.95	96.30	9.60	-86.70
RegNetX-400MF [51]	94.57	27.33	-67.24	94.38	19.18	-75.20
RegNetX-8GF [51]	97.14	40.76	-56.38	96.22	19.24	-76.98
RegNetX-16GF [51]	97.90	34.86	-63.04	95.84	13.34	-82.50

Y. Xu and P. Ghamisi, "Universal adversarial examples in remote sensing: Methodology and benchmark," *IEEE Trans. Geosci. Remote Sens.*, vol. 60, pp. 1−15, 2022.

UAE-RS Dataset

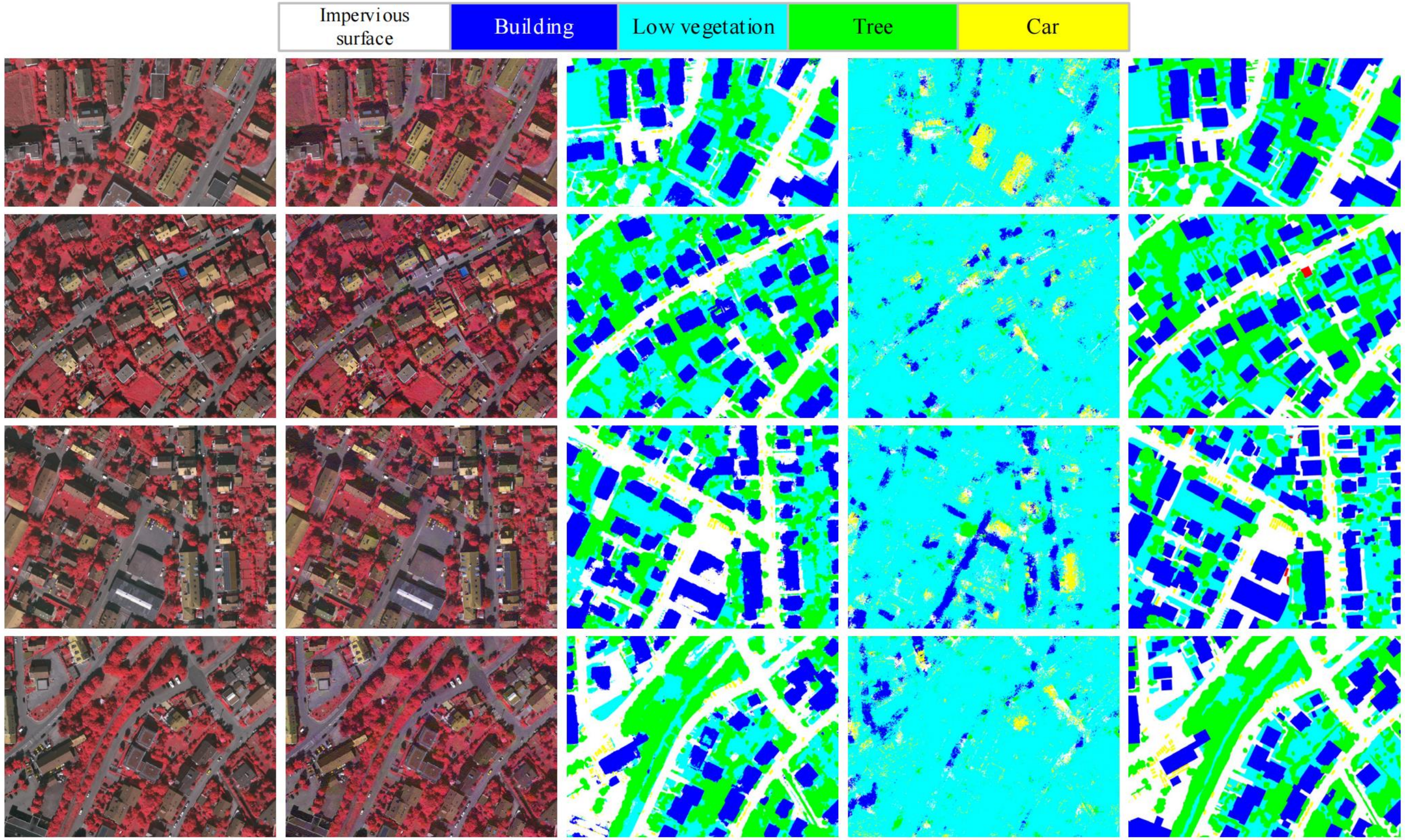

Qualitative results of the black-box adversarial attacks from FCN-8s → SegNet on the Vaihingen dataset

Y. Xu and P. Ghamisi, "Universal adversarial examples in remote sensing: Methodology and benchmark," *IEEE Trans. Geosci. Remote Sens.*, vol. 60, pp. 1−15, 2022.

Application

- AI for environmental monitoring

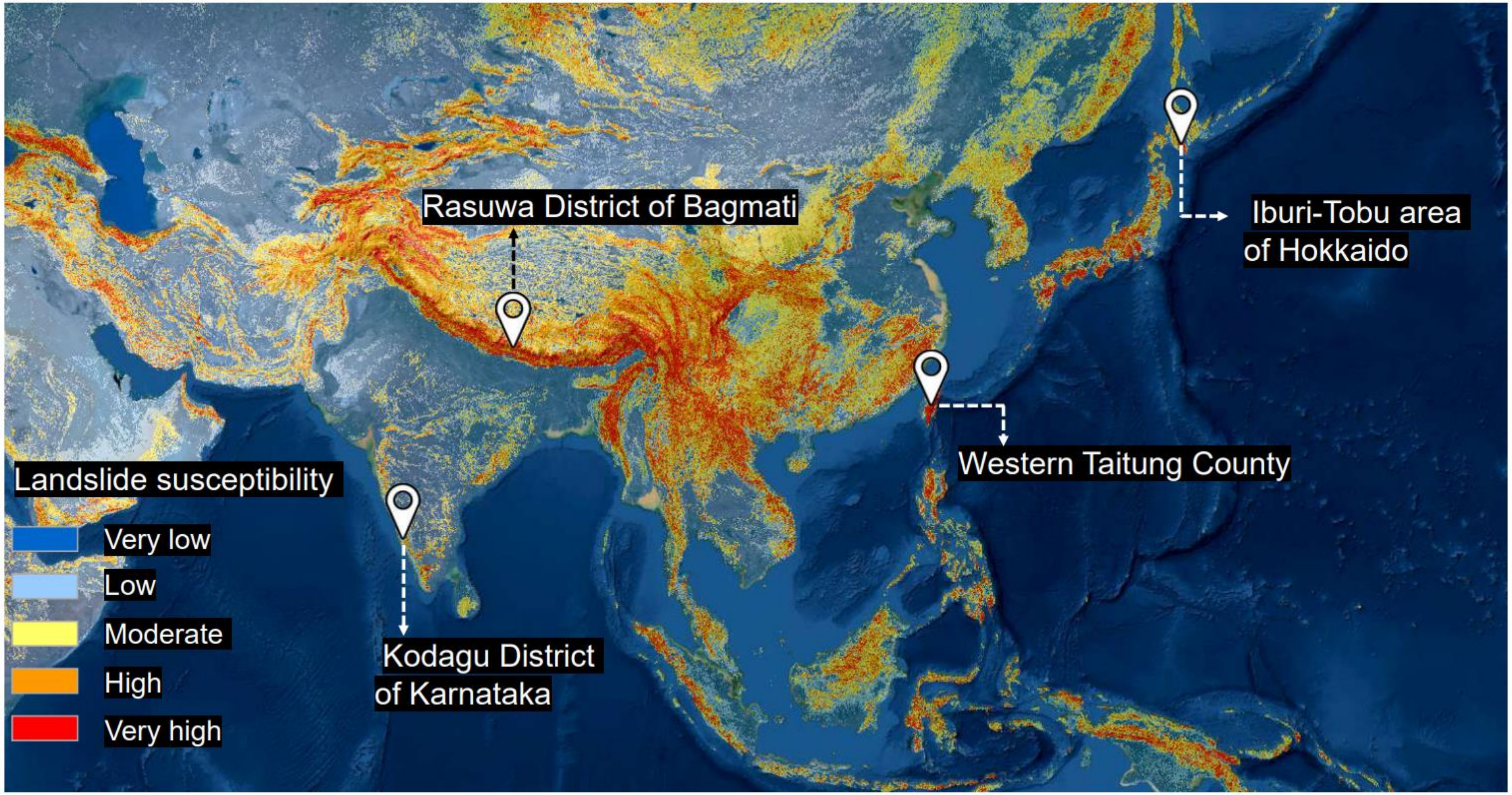

O. Ghorbanzadeh, Y. Xu, P. Ghamisi, M. Kopp, and D. Kreil, "Landslide4sense: Reference benchmark data and deep learning models for landslide detection," *IEEE Trans. Geosci. Remote Sens.*, vol. 60, pp. 1-17, 2022.

Application

- Satellite remote sensing for global wildfire observation

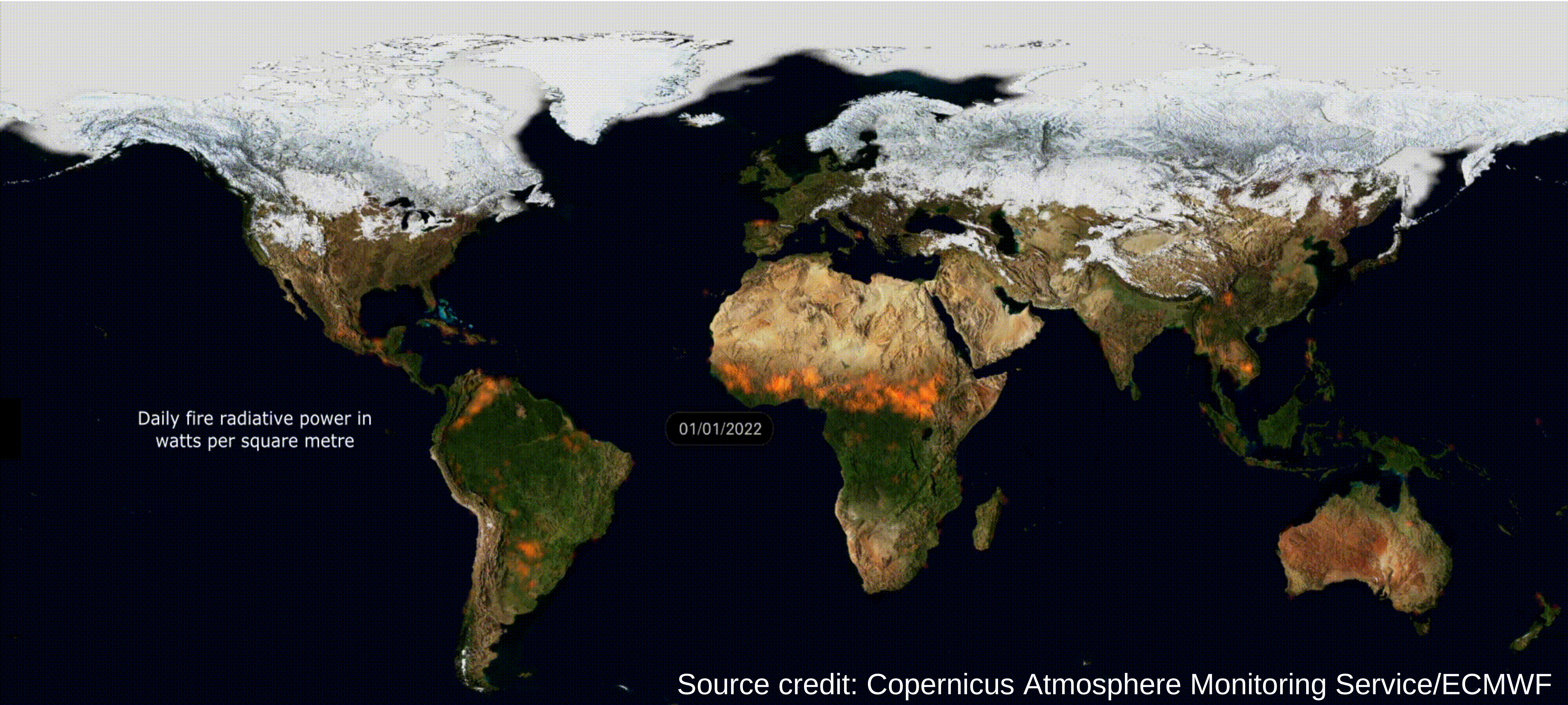

Source credit: Copernicus Atmosphere Monitoring Service/ECMWF

Application

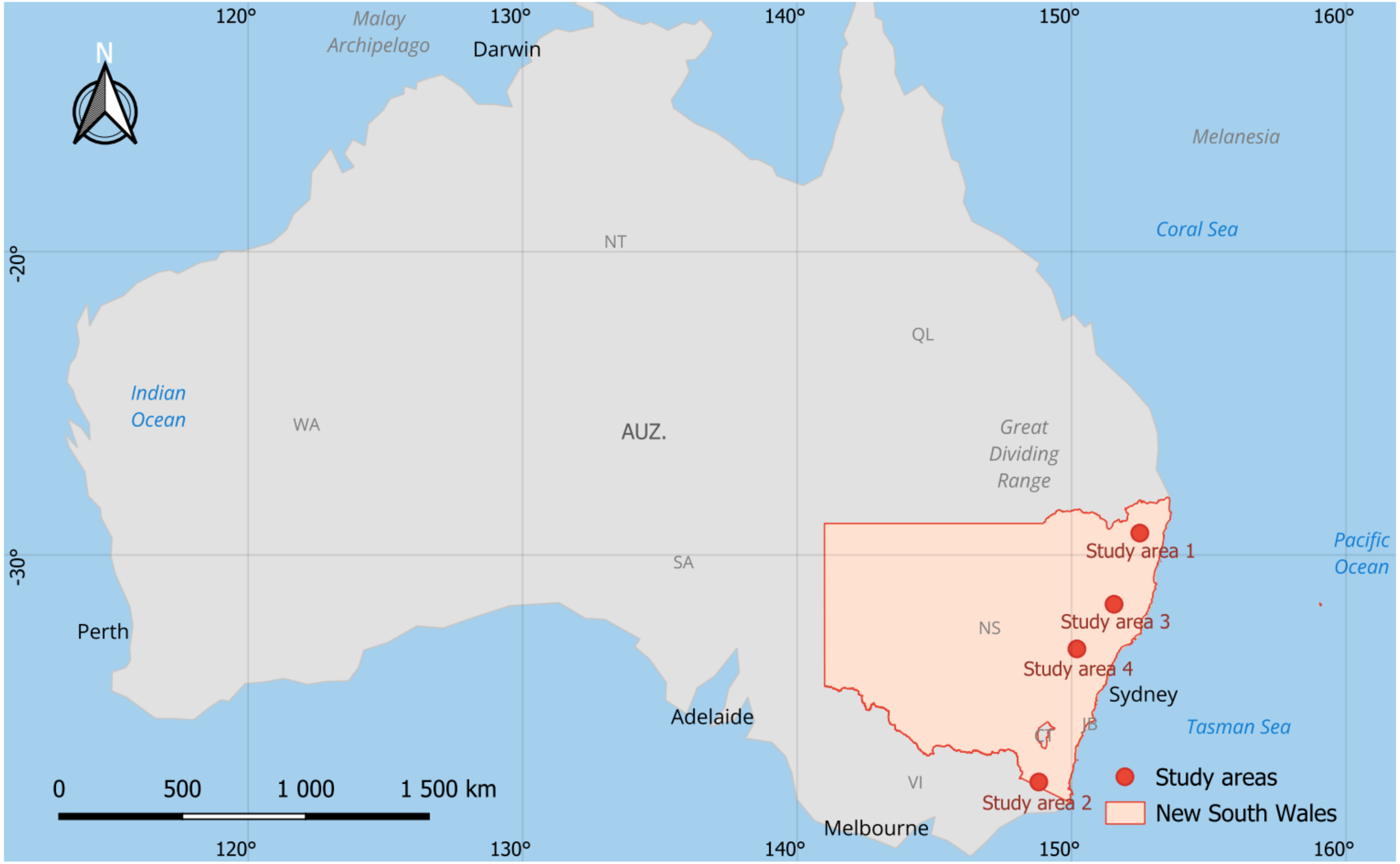

Sentinel-2

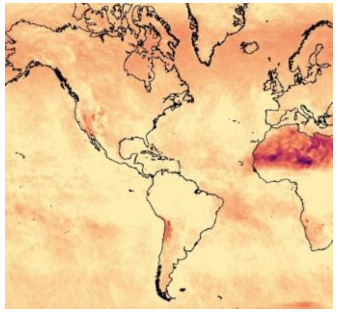

Sentinel-5P

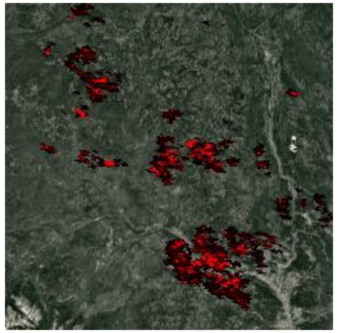

MOD14A1

Four bushfires happened in the 2019–2020 Australian bushfire season

LINKÖPING UNIVERSITY ELLIIT Excellence Center at Linköping – Lund in Information Technology

Y. Xu, A. Berg, and L. Haglund, “Sen2Fire: A Challenging Benchmark Dataset for Wildfire Detection using Sentinel Data,” *IGARSS*, 2024.

Data Information

Table 1. Band information in the *Sen2Fire* dataset.

	Sen2Fire bands	Central wavelength (μm)	Original resolution (m)
Sentinel-2	B1 – Coastal aerosol	0.443	60
	B2 – Blue	0.490	10
	B3 – Green	0.560	10
	B4 – Red	0.665	10
	B5 – Vegetation red edge	0.705	20
	B6 – Vegetation red edge	0.740	20
	B7 – Vegetation red edge	0.783	20
	B8 – NIR	0.842	10
	B9 – Vegetation red edge	0.865	20
	B10 – Water vapour	0.945	60
	B11 – SWIR	1.610	20
	B12 – SWIR	2.190	20
Sentinel-5P UV aerosol index product	B13 – Aerosol index	/	1113

LINKÖPING UNIVERSITY ELLIIT Excellence Center at Linköping – Lund in Information Technology

Sen2Fire Dataset

- Visualization

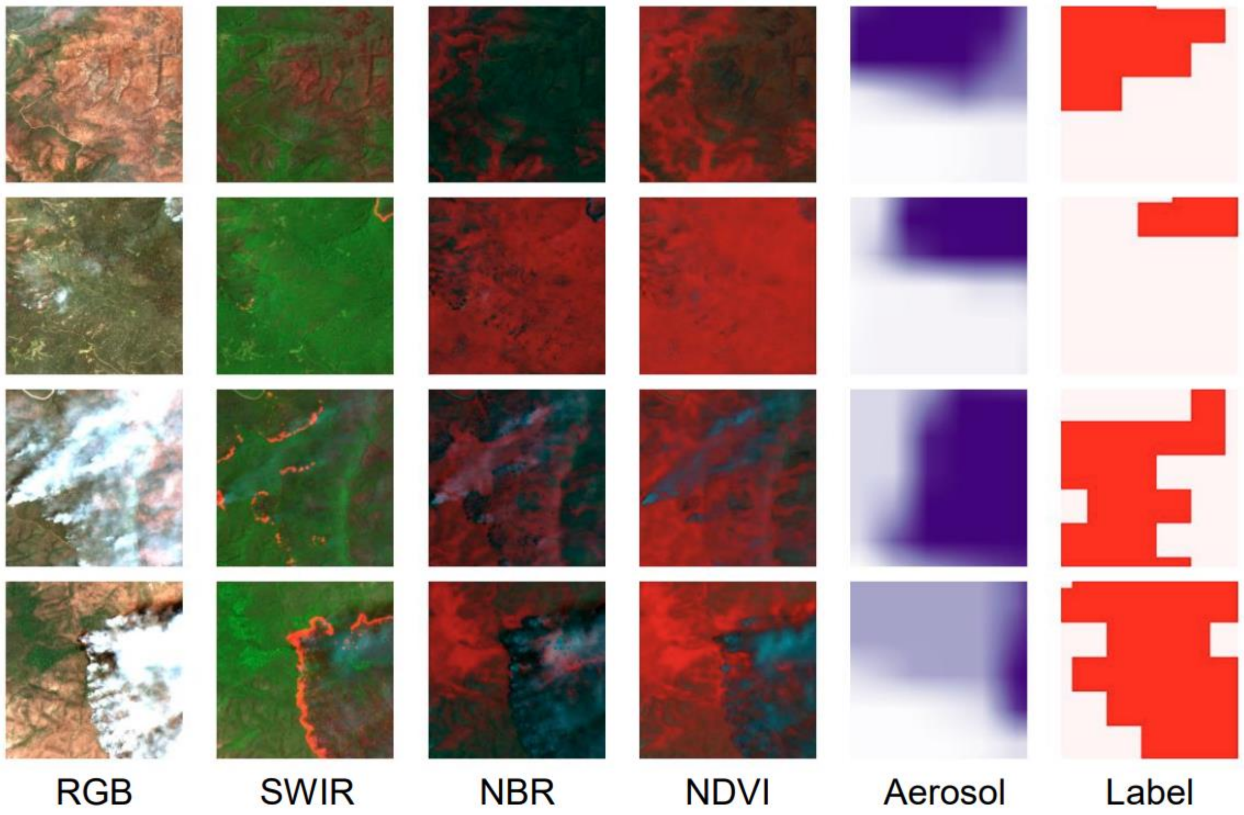

- Spectral Indices

Normalized burn ratio (NBR)

$$NBR = \frac{NIR - SWIR}{NIR + SWIR}$$

Normalized difference vegetation index (NDVI)

$$NDVI = \frac{NIR - Red}{NIR + Red}$$

Sen2Fire Dataset

Frequency Distribution

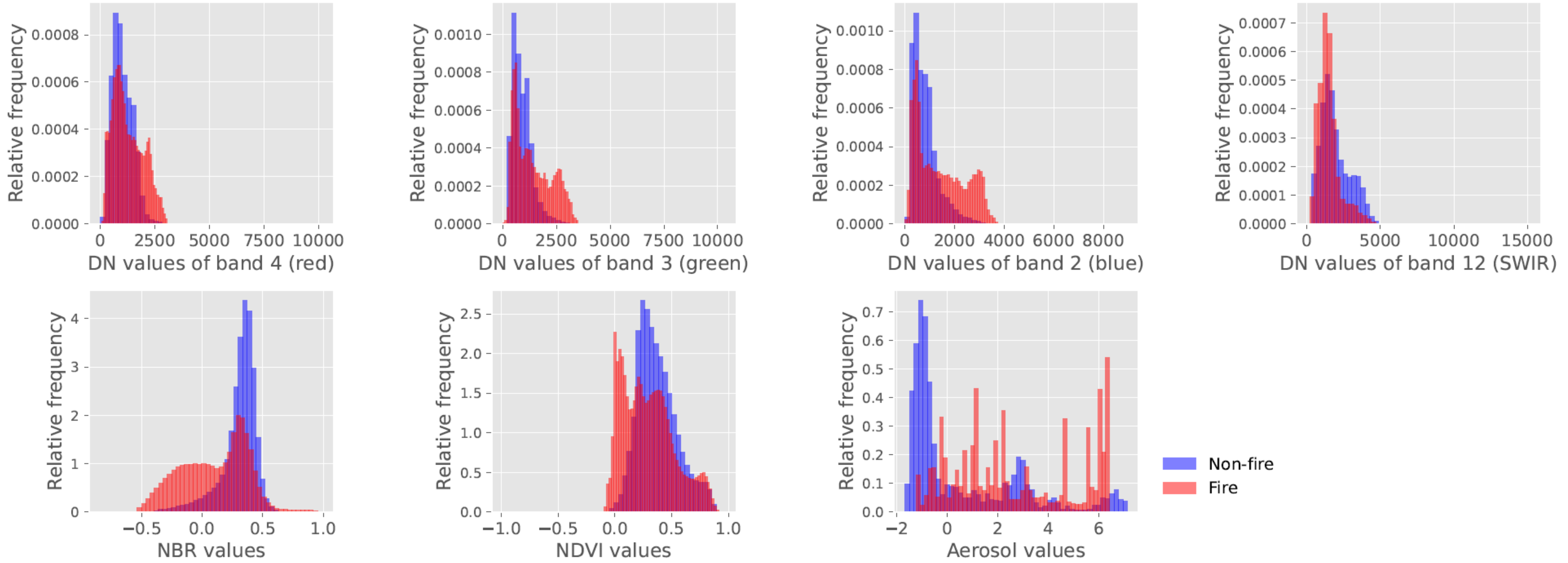

The relative frequency distribution of the digital number (DN), index, or aerosol values for fire and non-fire samples in the training set

Preliminary Experiments

- Input Strategies

RGB composite: B4,B3,B2.
SWIR composite: B12,B8,B4.
NBR composite: NBR,B4,B3.
NDVI composite: NDVI,B4,B3.
RGB+SWIR+NBR+NDVI: B4,B3,B2,B12,NBR,NDVI.
Vanilla input: B1,B2,B3,...,B10,B11,B12.

Input strategies	Precision	Recall	F1 score
RGB composite	11.8	18.3	14.4 (*)
+aerosol	14.7	21.3	17.4↑3.0
SWIR composite	43.9	20.5	27.9 (*)
+aerosol	39.7	21.8	28.1↑0.2
NBR composite	26.0	24.1	25.1 (*)
+aerosol	20.6	23.9	22.1↓3.0
NDVI composite	13.4	13.0	13.2 (*)
+aerosol	11.4	23.1	15.2↑2.0
RGB+SWIR+NBR+NDVI	38.6	17.1	23.7 (*)
+aerosol	35.5	19.1	24.8↑1.1
Vanilla input	22.4	29.5	25.5 (*)
+aerosol	37.4	20.1	26.1↑0.6

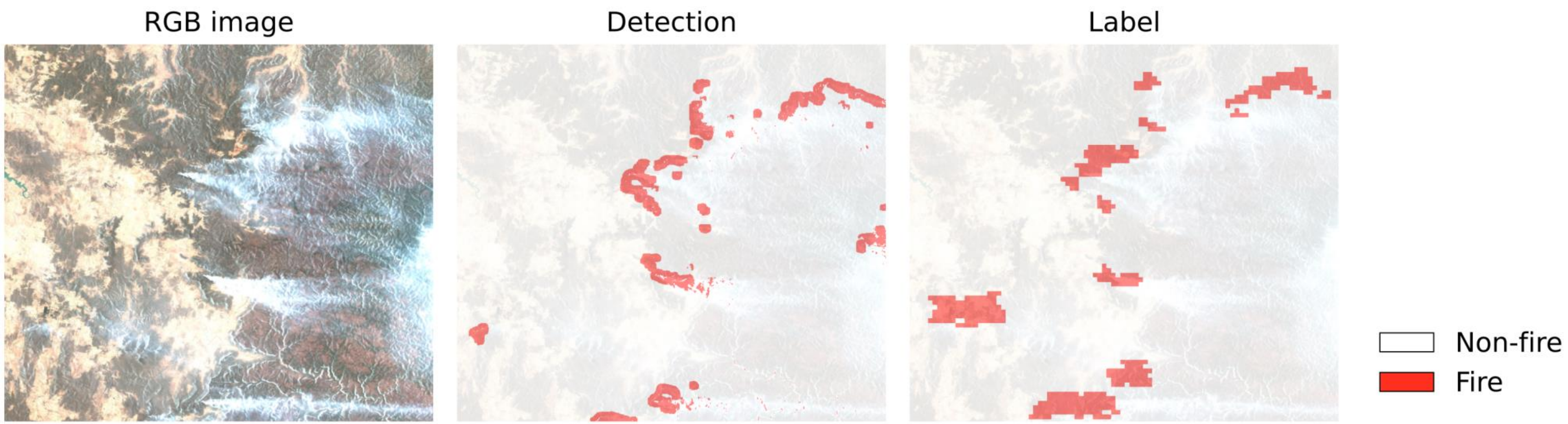

Wildfire detection result on the test set. The input patches are concatenated to reconstruct the complete image tile

Y. Xu, A. Berg, and L. Haglund, "Sen2Fire: A Challenging Benchmark Dataset for Wildfire Detection using Sentinel Data," *IGARSS*, 2024.

Application

- Satellite remote sensing alone is insufficient for early local fire detection

Application

- Satellite remote sensing alone is insufficient for early local fire detection

Application

- Satellite remote sensing alone is insufficient for early local fire detection

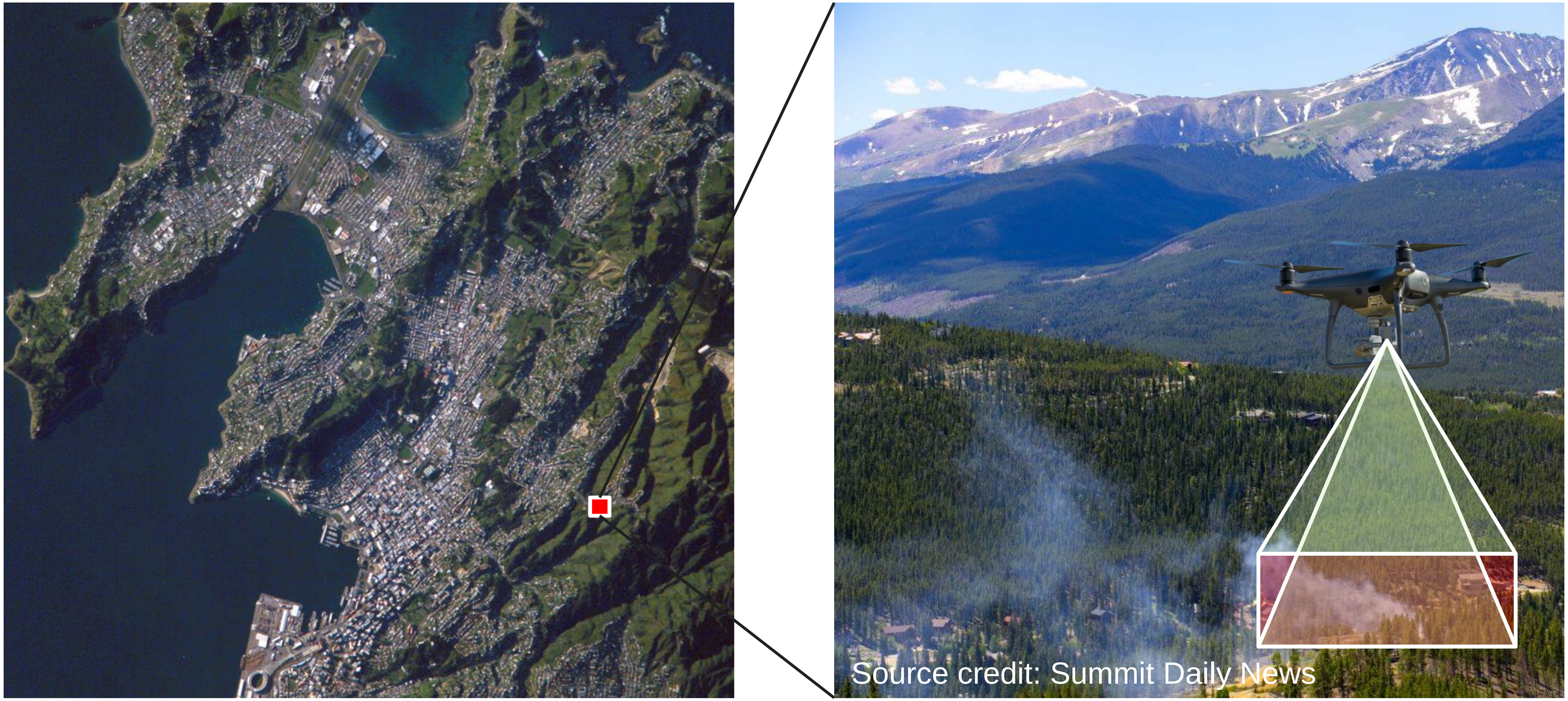

Dual-Camera AI

- Real-time autonomous wildfire detection system with dual-camera AI

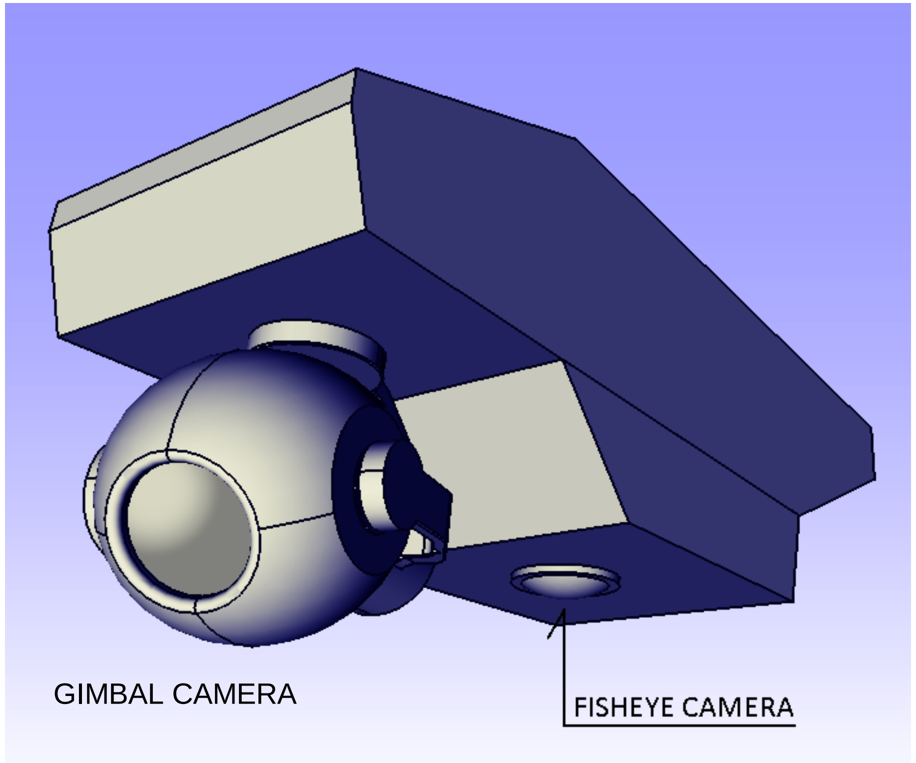

Dual camera system

The camera interface highlights regions of interest via a user or **a learnable detector**

Dual-Camera AI

- Real-time autonomous wildfire detection system with dual-camera AI

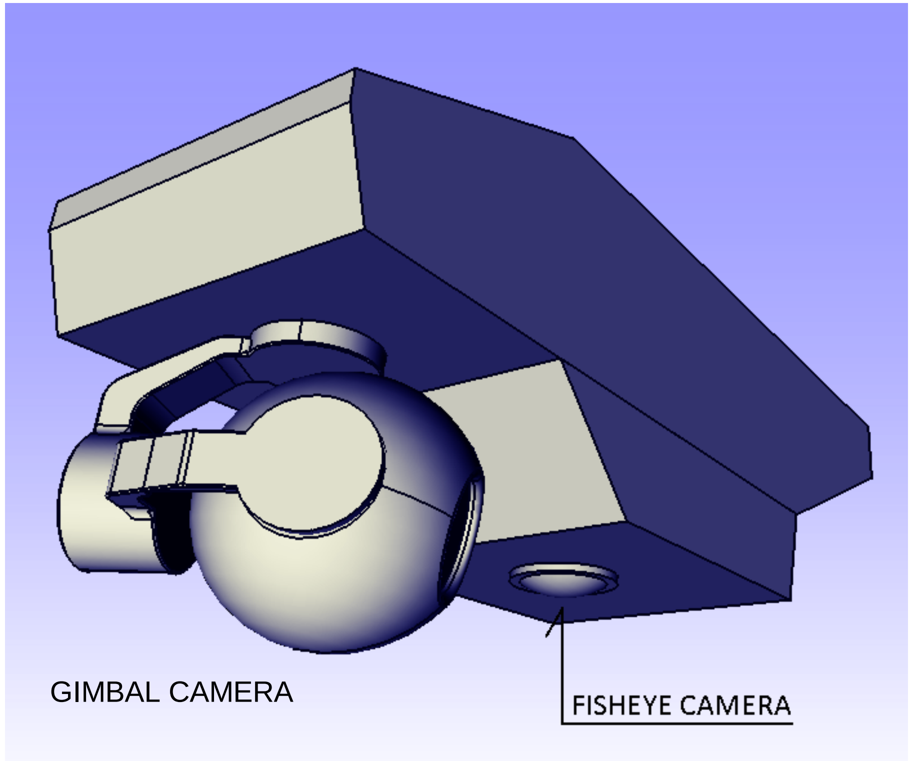

The gimbal panned to zoom in on the region of interest

The user receives a more detailed picture of the region of interest

LINKÖPING UNIVERSITY ELLIIT Excellence Center at Linköping – Lund in Information Technology

Future Direction

- Earth dynamics modeling

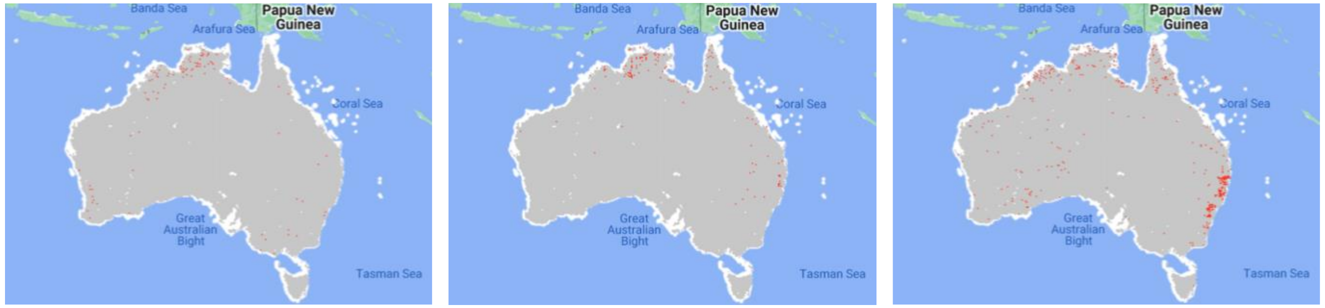

(a) April 2019 – June 2019 (b) July 2019 – September 2019 (c) October 2019 – December 2019

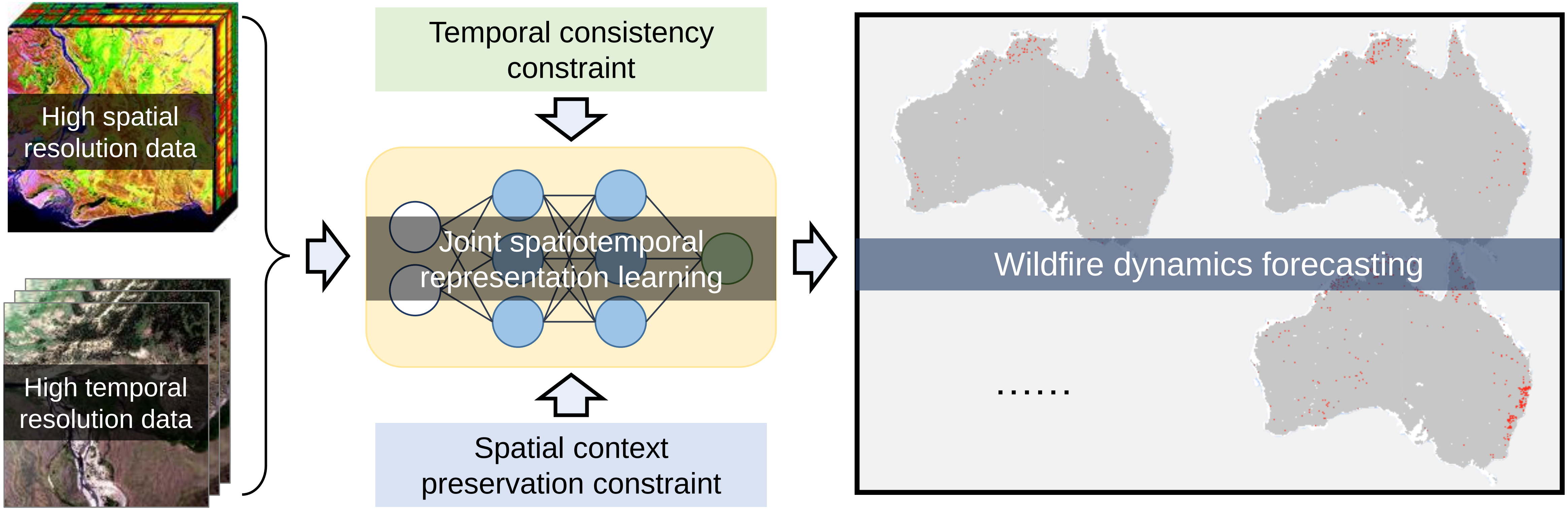

Thank You!

Yonghao Xu
Computer Vision Laboratory
Department of Electrical Engineering
Linköping University